Extended Atmospheres of Outer Planet Satellites and Comets

William H. Smyth

and

Michael R. Combi

Atmospheric and Environmental Research, Inc.
840 Memorial Drive
Cambridge, MA 02139-3794

November 1987

Interim Report for the Period
June 15, 1987 to September 14, 1987

TECHNICAL REPORT STANDARD TITLE PAGE

1. Report No.	2. Government Accession No.	3. Recipient's Catalog No.

4. Title and Subtitle	5. Report Date
Extended Atmospheres of Outer Planet Satellites and Comets	November 1987
	6. Performing Organization Code
7. Author(s)	8. Performing Organization Report No.
William H. Smyth and Michael R. Combi	
9. Performing Organization Name and Address	10. Work Unit No.
Atmospheric and Environmental Research, Inc. 840 Memorial Drive Cambridge, MA 02139-3794	11. Contract or Grant No. NASW-3966
	13. Type of Report and Period Covered Interim Report 6/15/87 - 9/14/87
12. Sponsoring Agency Name and Address NASA Headquarters Headquarters Contract Division Washington, D.C. 20546	14. Sponsoring Agency Code
15. Supplementary Notes	

16. Abstract

A major model documentation paper for cometary gas coronae and a second paper that successfully applied the model to simulate the hydrogen Lyman-α coma of comet Kohoutek were completed and are discussed. New and very exciting data for the hydrogen distribution in the Saturn system obtained from earlier unreduced Voyager 1 and Voyager 2 data are preliminarily reviewed. These new data open up a whole new series of investigations and indicate that Saturn's corona plays a major role in supplying hydrogen to the circumplanetary volume.

17. Key Words (Selected by Author(s))	18. Distribution Statement
satellites comets	

19. Security Classif. (of this report)	20. Security Classif. (of this page)	21. No. of Pages	22. Price*
Unclassified	Unclassified	4	

*For sale by the Clearinghouse for Federal Scientific and Technical Information, Springfield, Virginia 22151.

I. Summary of Research for the Third Quarter

Research activities during this quarter for comets have focused upon completing two major papers describing the gas coma of comets. Research activities for the hydrogen distribution in the Saturn system have concentrated upon assessing exciting new data uncovered in Voyager 1 and Voyager 2 data tapes. Originally scheduled work to perform preliminary Titan torus model calculations was therefore postponed.

1. Cometary Coma

Two major papers were completed this quarter and submitted to The Astrophysical Journal for publication. Both papers are attached in the appendix of this report.

The first paper is entitled "Monte Carlo Particle Trajectory Models for Neutral Cometary Gases. I. Models and Equations." This paper documents a new class of Monte Carlo particle trajectory models based upon physical processes of atoms and molecules in the coma. The model provides a new level of realism in predicting the spatial distribution of observed chemical species in cometary comae and in exploring the basic physics of the transition zone between true fluid-flow and free molecular flow.

The second paper is entitled "Monte Carlo Particle Trajectory Models for Neutral Gases. II. Spatial Morphology of the Lyman-α Coma." This paper successfully applies the general model of the former paper to simulate the hydrogen Lyman-α image for Comet Kohoutek and includes near perihelion one image representing an extreme case for collisional thermalization. The success of the model in this application is noteworthy.

2. New Observational Data for Saturn-System Hydrogen

A significant effort of the past two years has been extended in acquiring additional data to characterize the hydrogen distribution in the Saturn system. The main avenue to pursue this goal has been the collaboration effort established with D.E. Shemansky, who is a member of the ultraviolet spectrometer instrument team (UVS) of the Voyager spacecraft. In this period, a search of the magnetic tapes containing all pertinent UVS data of Voyager 1 and Voyager 2 was undertaken. The search has uncovered a significant amount

of new data that had not previously been reduced. In fact, this new data set is approximately 2.5 times larger than the old data set that was already reduced and published by the UVS team. A summary of the older published data and newly reduced data is given in Table 1.

There are a number of interesting aspects of the new data in Table 1 that deserve discussion. The most spectacular is that from the Voyager 1 post-encounter data an image of the H Lyman-α emission has been constructed at a viewing angle of ~25° to the orbit plane of Titan. The image indicates that the brightness distribution is not cylindrically symmetric as expected for a Titan torus alone. The brightness distribution between Saturn and Titan's orbit has a minimum at pre-dawn and a maximum in the vicinity of the dusk terminator line suggesting an asymmetric dayside hydrogen source for a large electroglow-driven planetary corona. In the less corona-dominated portions of the circumplanetary hydrogen, the presence of the Titan hydrogen torus can be distinctly identified. In addition to these data, the newly reduced Voyager 2 pre-encounter data provide the best one-dimensional data in the orbit plane. Combining the earlier published data and new data in the analysis of the H distribution with an appropriately developed model for the planetary corona and the Titan hydrogen torus model should provide a most interesting study. This study will be initiated here and continued in our renewal proposal to be submimtted to NASA early in the next quarter.

II. Program of Research for the Next Quarter

Research activities in the next quarter will focus upon (1) further assessing the new data for the hydrogen distribution in the Saturn system, and (2) integrating new plasma data for the planetary magnetosphere currently undergoing reduction by E.C. Sittler into the Titan torus model to improve the lifetime description of hydrogen.

Table 1

Voyager Spacecraft Data Available for Research on the Atomic Hydrogen Distribution in the Saturn System

Voyager 1 pre-encounter data

- Published Data: 14 days of one-dimensional scan data nearly parallel to the satellite orbit plane have been reported in the V1 30 day science report (Science 212, 201-211, 1981). These data were obtained at a range of ~ 2 x 10^7 km from Jupiter.

- New Data: Additional data of similar nature is available but the quality is uncertain. The reduction process should be repeated to include the additional data.

Voyager 1 post-encounter data

- Published Data: none

- New Data: Observations were obtained in mosaic scans across the system. All the data have been reduced for the first time in the past few months of 1987. The Voyager 1 post encounter trajectory is out of the solar system plane, and the data are obtained at an angle of ~25° to the orbit plane of Titan. An image of the system in H Lyman-α emission has been constructed but is not yet published. The data in this image were obtained over the period 1980 DOY 324-343 (6-25 days post encounter) at spacecraft planet ranges of 0.83 x 10^7 - 0.33 x 10^8 km. The integration time of the data set is 126 hours. Titan moves ~ 1.25 orbits during the 20 day observing period.

Voyager 2 pre-encounter data

- Published Data: Observations of one-dimensional scan data approximately normal to the satellite orbit plane were published in the V2 30 day science report (Science 215, 548-553, 1982).

- New Data: All usable observations for one-dimensional scan data approximately parallel to the satellite orbit plan have been reduced for the first time. The data were obtained in 1981 DOY 180-186, at ranges of 0.54 x 10^8 - 0.49 x 10^8 km. The integration time for this data set is 88 hours. These observations provide the best one-dimensional data in the orbit plane of Titan that were obtained by the Voyager spacecrafts.

Voyager 2 post-encounter data

- Post-encounter sequences were not obtained because of the lockup of the scan platform drive.

Monte Carlo Particle Trajectory Models for Neutral Cometary Gases.

I. Models and Equations

by

Michael R. Combi

and

William H. Smyth

Atmospheric and Environmental Research Inc.

840 Memorial Drive

Cambridge, MA 02139

October 1987

Abstract

The Monte Carlo particle trajectory models for the distributions of neutral gases in cometary atmospheres, developed in original form several years ago have been greatly extended and generalized. In a Monte Carlo particle-trajectory model (MCPTM) the spatial distribution of a neutral cometary species is determined by calculating the explicit trajectories of many individual particles following the chain of parent vaporization, coma outflow, photodissociations, collisions, and decay through the appropriate number of generations. The original inner coma model has been generalized and now includes: (1) solar radiation pressure, (2) isotropic ejection of daughters owing to excess photolysis energy, (3) radially variable parent outflow speed and gas temperature, (4) time (heliocentric distance) dependent source rate and lifetimes, (5) heliocentric velocity dependent lifetimes and excitation, (6) multiple collisions with the outflowing gas which includes both the effects on the observed species as well as the energy transfer (photochemical heating) delivered to the coma. An extended coma MCPTM has also been developed for application to the spatially extended atomic clouds (e.g. H, C, and O), which uses the generalized inner coma MCPTM for the source region and calculates explicitly the atom trajectories in three dimensions, including the relative heliocentric orbits of the nucleus and cloud atoms and heliocentric velocity dependent radiation pressure where important. In this paper the mathematical derivations of the various methods employed in the MCPTM are presented in detail, and its application to the calculation of the photochemical heating of the inner coma through the partial thermalization of cometary hydrogen atoms produced by the photodissociation of water is discussed.

I. Introduction

Models of the neutral comae of comets have generally focused on two extreme limits of actual conditions which occur in cometary comae. These are: (1) exospheric models which describe the distributions of particles in the outer coma where collisions between particles are rare, and (2) fluid based models which describe the bulk properties of various fluids (composed of molecules, atoms, dust etc.) that are to one extent or another collisionally coupled to each other or are at least self-coupled, and which are thus used to investigate such complex issues as gas-phase chemistry and/or dynamics.

The first models were simple exospheric models used to describe the observed distributions of gas and dust in the comae of comets. The fountain model of Eddington (1910) described the space and column density distribution for particles emitted isotropically from a point source (the cometary nucleus) moving under the influence of a constant radiation solar radiation pressure force. Further enhancements to the basic fountain model were added and are documented in the work of Wallace and Miller (1957). Perhaps the most notable contribution was that of Haser (1957,1966) whose models for radial outflow of a daughter species produced by the photodissociation of an unknown parent take into account either production and decay scale lengths or one scale length and radiation pressure acceleration. The two scale length model is still largely used today, despite many shortcomings, to analyze the observations of neutral radicals and atoms.

Models introduced by Keller and Thomas (1975) and Keller and Meier (1976) were isotropic point source models for application to the large spatially extended hydrogen coma as observed above the earth's atmosphere in the light of resonantly scattered solar Lyman-α. These models used the calculation of the syndyname on the sky plane to approximate the apparent distortion

introduced by the fact that the H atoms were actually following heliocentric orbits under the influence of solar gravity and solar radiation pressure. Meier et al. (1976) were able to use this model to analyze two-dimensional sky-plane images of comet Kohoutek (1973 XII). They required the use of the weighted superposition of three Maxellian distributions (with most probable speeds of 4, 8 and 20 km sec^{-1}) to describe the effective outflow speed distribution of H atoms from the inner coma region ($< 10^5$ km). Since the speed distribution resulting from the excess energy of the photodissociation of water (which based on circumstantial evidence was suspected to be the ultimate source of observed H atoms and OH radicals) was calculated to have a speed distribution sharply peaked at 8 and 20 km sec^{-1}, Meier et al. suggested that the thermalization of H atoms in the inner coma by collisions with heavy parent gas was responsible for the low speed atoms.

An important departure for the exospheric models took place with the introduction of models which take into account the (non-radial) isotropic ejection of daughter radicals (or atoms) upon photodissociation of the parent. In independent work using very different methods Combi and Delsemme (1980a) and Festou (1981a) developed new models which take into account this isotropic ejection. The main impetus behind this type of work was the fact that parent (source) scale lengths determined by applying Haser's model to the observed radial brightness distributions of cometary radicals were found to be generally smaller than values calculated using estimated cometary gas outflow speeds and photodissociation lifetimes computed from the solar uv flux and measured photoabsorption cross sections.

Combi and Delsemme (1980a) developed two approaches to this problem. One is the average random walk correction to the interpretation of Haser's model. The other is the explicit simulation of the isotropic ejection by

Monte Carlo methods. Their models were applied to the observed spatial distributions of CN in comets (Combi and Delsemme 1980b, Combi 1980). Festou (1981a) developed the vectorial model in which the isotropic ejection of photodissociated OH radicals from the outflowing H_2O molecules is explicitly solved for and numerically integrated. Both studies concluded that Haser's model though useful in describing the apparent distribution of observed radicals, underestimates the true scale lengths of true parent molecules.

More recently, Kitamura et al. (1985) have added a multiple collision algorithm to the basic Monte Carlo model of Combi and Delsemme (1980a). They have used their new model to begin the study of the collisional thermalization of cometary hydrogen atoms in the inner coma and conclude that collisions are important for the combination of small heliocentric distance and large gas production rate. Later in this paper we will return to the discussion of their work since we have considerably extended and improved their initial approach. It is important to note here that the addition of collisions to a basically exospheric model represents a first step toward modeling the transition zone between collision-dominated fluid flow and essentially collisionless free molecular motion. Bockelee-Morvan and Gerard (1984) and Schloerb and Gerard (1985) have also adopted the Monte Carlo method rather than the vectorial model, since they need to describe both the space density and the velocity distributions of OH necessary for interpreting 18-cm radio observations in comets.

The fluid-based models have been applied to the collision dominated inner coma. Originally, two types of modeling in this area had been developed. These were the pure hydrodynamic model and the Lagrangian gas-phase chemical model. In the pure hydrodynamic models the dynamics (flow speed and temperature) of the coma was the object of study. The paper by Mendis and Ip

(1975) gives an excellent review and a complete documentation of the early work in this area. The Lagrangian gas-phase chemical models assumed the coma could be described as a single fluid parcel traveling away from the nucleus in which non-equilibrium gas phase chemistry (in addition to photochemistry) could occur. Important examples of such models were developed by Giguere and Huebner (1978), Mitchell et al. (1981) and Cochran (1985). Typically these models contain the possible inclusion of many species (>100 including parent molecules and their fragment radicals, atoms and ions) and a large network of chemical and photochemical reactions (>1000). More recently, dynamics and chemistry have been combined in chemical gas-dynamic and dusty-gas-dynamic (Marconi and Mendis 1982, 1983, 1984; Huebner and Keady 1983; Ip 1983; Crovisier 1984; Gombosi et al. 1985). An excellent review article by Gombosi, Nagy and Cravens (1986) presents a detailed discussion of the methods and procedures involved in such models.

What typically distinguishes the models of different investigators from one another is the extent to which different processes are included and by what methods they are included, for example: IR, visible and UV radiative transfer, gas-phase chemistry, radiative cooling, photochemical heating, multiple fluids for various classes of gas species, electrons, ions and dust, and finally full time-dependent dynamic equations. Even two dimensional axisymmetric dusty-gas models have been developed to study the evolution of gas and dust jets (Kitamura 1986, and Komle and Ip 1986).

As mentioned earlier the fluid based models are applicable deep in the collision zone where the gas can reach thermal equilibrium and can be described at any point in space as one or more fluids (being coupled or not) each having in general a bulk velocity and one or more temperatures (i.e., kinetic and internal states). Departures from local radiative equilibrium

have been treated by iterative methods in most of the gas-dynamic models (see references above). However, when the collisional mean free path for molecules becomes too large the applicability of a hydrodynamic model breaks down even for the flow mechanics. The gas in these models is described in terms of a phase space distribution consisting of a bulk motion and a kinetic temperature. A sufficient collision rate is required in order to constantly re-equilibrate a Maxwell-Boltzmann distribution and eventually transfer this internal energy to bulk flow through adiabatic expansion. The free-flow exospheric models are applicable in the outer regions where essentially no collisions between molecules occur. A characteristic distance separating these two regions is typically defined such that the distance to the nucleus is equal to the local mean free path for intermolecular collisions. This distance called the collision zone radius, is the direct analogue to the exobase level in planetary atmospheres (Chamberlain 1963).

Figure 1 shows the collision zone radii for a number of representative comets as a function heliocentric distance, as estimated from published gas production rates and/or visual light curves. It is seen that the collision zone radius can vary from values of less than 100 km (as will be expected for much of the time CRAF will be in the vicinity of comet P/Tempel 2) to values greater than 100,000 km for comets Kohoutek and West near their perihelion times. For much of the time extensive ground-based observations were made of comet P/Halley (0.6 - 2 AU) the collision zone radius was of order one to a few tens of thousands of km. Also plotted in Figure 1 are several values of the percentage of water photodissociated as a function of distance from the center of the nucleus and of the heliocentric distance. What is critical here is that the higher the percentage of water dissociated within the collision zone, the higher the heating rate and the larger the extent of hydrogen atom

thermalization will occur. The simple relation between the collision zone radius and the water photodissociation scale length is complicated by the large mass ratio between the hot freshly produced H atoms and the outflowing heavier gas atoms and molecules so many collisions are required to thermalize the H atoms completely. Therefore, comparison of collision zone radii and percentage of water photodissociation only provides an upper limit to the heating and thermalization.

In reality, there is no clear separation between the inner (collisional) and outer (collisionless) regimes, and a large transition region exists at distances of order of the collision zone radius. For the less productive periodic comets (P/Encke and P/Tempel 2), it appears fairly clear that an exospheric (free-flow) model is in fact applicable to the generally observable comae and that the fluid dynamic models are only applicable out to a few tens of km at best. However for the large productive comets, fluid models should be applicable in a much larger inner coma (perhaps a few thousand km), but typical distances of importance to observations are made right in the middle of the transition region. Furthermore, even in the case of the planetary exobase where, owing to the presence of gravity and the exponential decrease in density with increasing height, the transition from a fluid to a collisionless corona is much more spatially confined, the applicability of a thermalized Maxwell-Boltzmann distribution is questionable (Fahr and Shizgal 1983). In the case of a cometary atmosphere the density decreases approximately with an inverse square law so the transition is much more gradual.

The Monte Carlo particle trajectory model (MCPTM) allows us to bridge the gap between the regimes of the purely fluid to the purely free flow models and to investigate the conditions in this all-important transition region. In

fact, the MCPTM provides the only reasonable way to describe accurately the appropriate space-time-velocity distributions for molecules, radicals and atoms even in otherwise purely free flow models, owing to such complications as solar radiation pressure, orbital motion effects, time dependences, noniso-tropic production, and correct inner coma outflow conditions.

In the remainder of this paper we will describe the mathematical formalism used in the application of the principle of Monte Carlo to a wide variety of processes in the cometary atmosphere. Section II describes the basic procedures used in the inner coma model. Section III describes the geometrical and orbital mechanics procedures for the extended coma model. Section IV describes a particular application which couples a steady-state inner coma MCPTM with a simple gas-dynamic model to study the photochemical heating of the coma by the thermalization of photodissociated hydrogen atoms. Section V presents a summarized discussion of the implications of the MCPTM, its capabilities, as well as future work to be pursued in this area. The companion paper to this one (Combi and Smyth 1987b hereafter called Paper 2) describes in detail the coupled aspects of the thermalization of hydrogen atoms as it relates to the spatial morphology of the observed two-dimensional distribution of the Lyman-α coma and to the dynamics of the inner coma. Some of the results of using the MCPTM have been described previously (Combi and Smyth 1985, Combi, Stewart and Smyth 1986, Combi 1987, and Combi and Smyth 1987a), however, most of the mathematical and numerical details concerning the MCPTM appear only in this and the companion paper in this issue.

II. Monte Carlo Methods for the Inner Coma Source Model

The original application of the Monte Carlo method to describe the spatial distribution and kinematics of neutral gases in cometary atmospheres was discussed by Combi and Delsemme (1980a). Further refinements and additions have been discussed by Bockelee-Morvan and Gerard (1983) and Kitamura et al. (1985). In this section of the paper we present a number of fundamental model advances, some of which are in the interest of model efficiency or improved statistics (such as the use of skewed probability density distributions and appropriate weights, or forced dissociations), while others are to add generalizations or new physical processes (such as time dependent lifetimes, Maxwell-Boltzmann distributions, or multiple particle collisions). In all applications the Monte Carlo method is used by computing the actual trajectories of many ($\sim 10^5$) radicals or atoms, making sure that all of the important variables (time, space, velocity etc.) are appropriately spanned, and then calculating space and column densities, and radiative emission rates by explicitly counting the total weighted numbers of particles (radicals or atoms) within regions of specified volume and area, respectively. Similarly, doppler profiles can be computed by also counting particles in specified line-of-sight velocity bins.

In all situations, the principle of Monte Carlo is used to span the possible states a particle may occupy relative to some variable or condition. These variables or conditions can be related to the weight associated with a particle, owing to production rate variations, or source and decay lifetimes, or they can relate to the trajectory calculations, owing to isotropic redirection upon dissociation or collision, or a thermalized speed component. Many of the derivations in this paper are direct analogues or extensions of processes outlined in a monograph by Cashwell and Everett (1959), which was written to

address a number of problems in photon and neutron scattering in bulk material having complex geometrical configurations. In order to use the Monte Carlo method, a state or property of a particle, defined symbolically as x', must be charcterized in terms of a probability density distribution function, p(x')dx'. A probability distribution function can then be defined such that $P(x) = \int_{x_1}^{x} p(x')dx'$, on some interval from x_1 to x_2. If the probability density is properly normalized on this interval, then $\int_{x_1}^{x_2} p(x')dx'=1$, and values, x_i, of the distribution can be spanned according to the relation

$$P(x_i) = \int_{x_1}^{x_i} p(x')\ dx' = R_i \tag{1}$$

where R_i is a uniformly distributed set of numbers on the interval $0 \leq R_i < 1$. Typically in a computer simulation, the values, R_i, are supplied by a suitable pseudo-random number generator on the interval from 0 to 1. A large sample of the variable is then found by solving for x_i in Eq 1 for many random numbers.

In a Monte Carlo coma simulation the object is to build up the complete distribution of the observed species (atoms or radicals) in space at some absolute observation time, t_{obs}. In order to accomplish, this parent molecules are emitted from the nucleus during a long time interval of length t_f, preceeding t_{obs}. For a constant production rate (a steady-state model), the density distribution function which describes the emission times for parent molecules is constant; in other words all emission times are equally probable. Equivalently, all emission backup times before the observation time, t_{obs}, are equally probable. Therefore, as in the original Monte Carlo model (Combi and Delsemme 1980a), individual parent molecules are emitted from the nucleus at many backup time intervals, t_i, distributed randomly on the complete coma buildup time interval, t_f. This results in a simple application

of the Monte Carlo method so that the parent production backup time intervals are given simply as $t_i - t_f R_i$. For an isotropic point source the initial parent molecule ejection direction is defined in terms of the standard spherical polar and azimuthal angles (θ_i and ϕ_i) as $\cos \theta_i = 1 - 2R_i$ and $\phi_i = 2\pi R_i$, where a different random number is used for each angle. In these simple cases the probability density function is constant and the application of the Monte Carlo method is trivial.

Certain processes like those just mentioned can be characterized as an even distribution, e.g., for a steady state vaporization rate all production times are equally probable. Even for case of dissociation with a constant lifetime all population probabilities are equally probable (Combi and Delsemme 1980a). However, owing to overall poor statistics resulting from the modeling of a relatively rare event such as a dissociation, it is desirable to force the event to occur in a specified amount of time and penalize the resulting particle by only counting a fractionally weighted particle. Similarly, an uneven statistical coverage in the output bins, which results when the radial space and column density bins are distributed logarithmically in distance from the nucleus, can be compensated for by skewing the known probability density distribution in time and then by correctly weighting the final particle. In our current MCPTM we use both the procedures of forced dissociation and that of skewed production and dissociation time distributions to make the model much more efficient, and also introduce the inclusion of time-dependence in molecular lifetimes.

In the original steady-state procedure, a decay time interval, t_D, was computed using the principle of Monte Carlo, which yields the relation $t_D = -\tau \ln (1-R_i)$ where τ is the exponential decay lifetime. This was computed twice, once for the parent and once for the daughter; a daughter

trajectory was only computed if the parent decay occurred within the backup time interval t_i and the daughter decay did not. A better method is to use the concept of a forced dissociation for the parent and a weighting function for the daughter decay (see forced first scattering discussion by Cashwell and Everett 1959). To force a parent dissociation within the backup time interval t_i, the probability distribution is renormalized within that interval, and the dissociation time interval is given by

$$t_D = -\tau \ln \left[1 - R_i \left[1 - e^{-t_i/\tau}\right]\right] , \tag{2}$$

and the particle is assigned a weight ($\neq 1$) given by

$$w_D = \left[1 - e^{-t_i/\tau}\right] , \tag{3}$$

where τ is the parent decay lifetime. The weight, w_d, of the daughter from its own exponential decay is given by

$$w_d = e^{-(t_i - t_D)/\tau_d} , \tag{4}$$

where τ_d is the daughter decay lifetime.

In the time-dependent model, the variable production rate is treated quite simply by weighting (w_Q) a parent molecule, according to the production rate at the emission time ($t_{observation} - t_i$) relative to the production rate at some standard time, e.g., at the observation time or at a comet heliocentric distance of 1 AU. Thus a water vaporization curve or a simple power law in heliocentric distance can be assumed; for that matter, transient activity or outbursts can also be accounted for by simple weighting.

The variable lifetime for the parent and daughter decay are somewhat more involved. The generally time-dependent lifetimes $\tau = \tau(t)$ can be approximated as a set of finite element steps

$$\tau = [\tau_1(T_1),\ \tau_2(T_2),\ \tau_3(T_3),\ \ldots,\ \tau_n(T_n)]$$

where $(T_1,\ T_2,\ T_3, \ldots T_n)$ are sub-intervals in time such that

$$T_1 + T_2 + T_3 + \ldots + T_n = t_i .$$

The partial weight associated with the forced dissociation is then given by

$$w_D = 1 - \exp[-(T_1/\tau_1 + T_2/\tau_2 + T_3/\tau_3 + \ldots + T_n/\tau_n)] \ . \tag{5}$$

The probability for a dissociation somewhere on this interval $0 \le t_D \le t_i$ is

$$P(t_D) = 1 - e^{-\rho} \tag{6}$$

where

$$\rho = \frac{T_1}{\tau_1} + \frac{T_2}{\tau_2} + \ldots \frac{T_{m-1}}{\tau_{m-1}} + \frac{t_D - (T_1 + T_2 + \ldots + T_{m-1})}{\tau_m} \tag{7}$$

and

$$T_1 + T_2 + \ldots + T_{m-1} \le t_D \le T_1 + T_2 + \ldots + T_m \ (m \le n) \ .$$

The quantity, ρ, is just the number of mean free times (like mean free paths) contained in time t_D.

Just as in the steady-state case, the random number enters as the fraction of parents dissociated until the time t_D; therefore,

$$R_i = (1 - e^{-\rho})/w_D \tag{8}$$

and solving for ρ we have

$$\rho = -\ln (1 - R_i w_D) \ . \tag{9}$$

Finally, t_D is determined from the inequality

$$\frac{T_1}{\tau_1} + \frac{T_2}{\tau_2} + \ldots + \frac{T_{m-1}}{\tau_{m-1}} < \rho \leq \frac{T_1}{\tau_1} + \frac{T_2}{\tau_2} + \ldots + \frac{T_m}{\tau_m} \tag{10}$$

and the equation

$$t_D = T_1 + T_2 + \ldots + T_{m-1} + \tau_m \left[\rho - \left(\frac{T_1}{\tau_1} + \frac{T_2}{\tau_2} + \ldots + \frac{T_{m-1}}{\tau_{m-1}}\right)\right] \ . \tag{11}$$

Once t_D is determined, the daughter decay partial weight can be calculated in a more straightforward manner by simply summing up the partial exponential weights for the remaining intervals from T_m up to T_n.

$$w_d = \exp - \left[\frac{\tau_m\left(\frac{T_1}{\tau_1} + \frac{T_2}{\tau_2} + \ldots + \frac{T_m}{\tau_m} - \rho\right)}{\tau_m\ (\text{daughter})} + \frac{T_{m+1}}{\tau_{m+1}(\text{daughter})} + \ldots + \frac{T_n}{\tau_n(\text{daughter})}\right] \ . \tag{12}$$

The final weight associated with the daughter is found simply by the product of the partial weights, $w_Q w_D w_d$.

The above discussion is appropriate for treating the true probability density functions. For the case of modeling the inner coma it is highly desireable to skew both the parent molecule production times and all dissociation times to small values. In the inner coma model radial distance bins are typically distributed logarithmically, and in the application of the inner coma model to the question of the computation of photochemical heating it is especially important to insure constant statistical certainty in all radial bins even those in the innermost coma. In order to understand the consequences of incorporating a skewed probability density distribution it is best to return to the basic probability density distribution function description of the Monte Carlo principle Eq.1. In the applications of interest for the coma MCPTM (either production time or dissociation time) it is convenient to construct a generalized state variable, η, for the process such that the probability density distribution function can be defined as $p(x)dx = d\eta$ and the solution for the principle of Monte Carlo (Eq.1), is then simply given by ${}_0\int^{\eta_i} d\eta = R_i$, which yields $\eta_i = R_i$.

For the case of uniform parent molecule production times the state variable is given by $\eta_i = t_i/t_f$; for constant dissociation lifetimes the state variable is $\eta_i = (1-e^{-t_D/\tau})/(1-e^{-t_i/\tau})$. When each of these definitions is equated to R_i and solved for t_i and t_D one finds, as expected, that $t_i = t_f R_i$ and that t_D is given by Eq 2. After trying a number of functional forms we found the best way to skew the resulting distributions toward smaller values of t_i and t_D was to require a distribution of the state variable of the form $\int_0^{x_i} p(x)dx = \eta_i = R_i^n$, where n is a positive number. It can be shown that a

normalized skewed probability density distribution function of the state variable of the form

$$p_s(\eta)d\eta = \frac{1}{n}\,\eta^{(\frac{1}{n} - 1)}\,d\eta \tag{13}$$

when integrated from 0 to η_i, results in the desired distribution. However, since this is not the true flat distribution in the appropriate state variable, a corresponding fractional weight must be included when the particle is counted in the model. Since the true physical distribution is flat then the appropriate weight for the skewed distribution of some value of the state variable, η, is found simply by the inverse of the probability density at that value. This is

$$w = n\eta^{(1-\frac{1}{n})} . \tag{14}$$

The weights for the skewed production time distribution, w_i, and the skewed dissociation time distribution, w_D, are

$$w_i = n\,(\frac{t_i}{t_f})^{(1-\frac{1}{n})} , \tag{15}$$

and

$$w_D = n\left(\frac{1-e^{-t_D/\tau}}{1-e^{-t_i/\tau}}\right)^{(1-\frac{1}{n})} . \tag{16}$$

In the final model output bins, each particle is counted as a weight and all particles contribute. The total weight is set by the product of several partial weights: w_Q for the production rate, w_i for the skewed production time

distribution (Eq 15), w_D for the forced dissociation (Eq 5 or 16), and w_d for the decay of the particle itself (Eq 4 or 12). The value of n in Eqs. 13-15 can be adjusted to produce the desired even statistical coverage in all output bins. A value of 3 has been found to produce reasonable results when a value for the total model run time for building the observable coma, t_f, is typically chosen to be at least 7 times the particle (radical or atom) lifetime.

Most of the discussion to this point has dealt with using the Monte Carlo method to compute the weight associated with a particle that results from its production and decay mechanisms. There are also Monte Carlo applications associated with the trajectory calculation of the particle. In current versions of the MCPTM these applications include: (1) speed distributions from excess photolysis energy, (2) Maxwell-Boltzmann distributions for the convective Maxwellian description of an outflowing coma having a specific temperature distribution, (3) multiple collisions of suprathermal particles (radicals or atoms) produced by the excess photolysis energy, and (4) random ejection directions after dissociation or collision. The method for generating random ejection directions was given by Combi and Delsemme (1980a) and mentioned again at the beginning of this section.

Simulating speed distributions (either known or assumed) is a simple and direct application of the Monte Carlo method (Eq. 1). In the case of an assumed or calculated speed distribution which is imparted on a particle (atom or radical) upon photodissociation of its immediate parent (radical or molecule) there is generally no known analytic form. So a numerical look-up table is generated from the speed probability density distribution function, f(v)dv, using Eq. 1, appropriately replacing p(x) by f(v), and integrating and solving for v_i to form the function, $v_i=v(R_i)$, in

$$\int_0^{v_i} f(v)dv = R_i \quad . \tag{17}$$

An example is illustrated in Figure 6 of Paper 2 for the case of the production of hot H atoms by the photodissociation of water molecules as derived from the results of Festou (1981b). In many cases, however, as for CN (Combi 1980), and for C_2 (Combi and Delsemme 1986), we assume an average monoenergetic speed.

Since the outflow of the coma gases is more realistically described by a bulk radial speed and some radially dependent temperature we have included a convected Maxwellian, and the simulation thereof, as an important mechanism in the MCPTM. It is especially important in the case of the photochemical heating calculation and the resulting speed distribution of the partially thermalized H atoms produced in the photodissociation of water. At some point in the coma, the gas flow of a parent molecule can be characterized by a temperature, T. The speed distribution, f(v) dv, of molecules of mass, m, at temperature T is given by the Maxwell-Boltzmann distribution,

$$f(v)\ dv = \frac{4}{\pi^{1/2}} \frac{v^2}{v_m^3} \exp\left[-\frac{v^2}{v_m^2}\right] dv \quad ,$$

where v_m is the most probable speed,

$$v_m = (2kT/m)^{1/2} \quad . \tag{18}$$

In order to simulate this speed distribution on a microscopic level with the particle-trajectory model, we can again use the principle of Monte Carlo (Eq. 1). Since the Boltzmann distribution is a normalized probability

density function, a simulated distribution can be generated from a random number sequence, R_i on the interval from 0 to 1 by solving for v_i in the equation,

$$\frac{4}{\pi^{1/2}} \frac{1}{v_m^3} \int_0^{v_i} v^2 \exp(-v^2/v_m^2)\, dv = R_i \quad . \tag{19}$$

The integral in this equation is not analytical, but can be transformed into a single parameterized function by making the substitutions: $u = v/v_m$, $u_i = v_i/v_m$ and $du = \frac{1}{v_m} dv$. The equation then becomes

$$\frac{4}{\pi^{1/2}} \int_0^{u_i} u^2 e^{-u^2}\, du = R_i \quad , \tag{20}$$

which has been numerically solved and included as an interpolated table of the form, $u_i = u(R_i)$, in the model.

The final application of the Monte Carlo method to be discussed here is that for collisions between the particles (atoms or radicals) and the background outflowing coma gas. As discussed in section I, Kitamura, et al. (1985) have published the first attempt of performing such a calculation as it applies to the thermalization of hot H atoms produced by the photodissociation of water molecules. Although we have followed their basic derivation of the application of the Monte Carlo method to the collision path, two of their assumptions regarding the conditions and density of outflowing coma can be improved. One is their assumption of a monoenergetic constant outflow speed for the coma. The other is their description of the density in the outflowing coma to be simply that for primary water molecules whose population decreases both (correctly) as the inverse square of the distance from the center of the

nucleus and also (but incorrectly) with the exponential scale length for the photodestruction of water.

The first improvement is to consider the coma to be described with a variable outflow speed and a variable temperature. Even for rather small values for the coma temperature, the thermal speeds of H atoms are generally at least comparable and possibly even several times larger than the typical values for the outflow speed (~1 km s^{-1}). Kitamura et al. (1985) dealt strictly with the effect of the outflowing gas on the final distribution in space and velocity of the H atoms. Although this is an important concern, we are also concerned with the heating effect of the hot H atoms on the coma. They have assumed a form for the description of the outflowing coma and performed a Monte Carlo multiple-collision simulation to calculate the H atom trajectories. We have found that the MCPTM can be used to calculate the photochemical heating which when coupled iteratively to a gas-dynamic model yields the outflowing coma description (i.e. the radial dependence in the gas temperature and outflow speed). As is shown in Paper 2, this coupled approach can be used to generate a self-consistent picture of the spatial morphology of the H Lyman-α coma and the inner coma conditions. More detailed discussions of these issues is presented in section IV of this paper and in Paper 2.

The second improvement, in addition to providing a better physical description of the coma, actually simplifies the collision calculation significantly. Kitamura et al. (1985) assume that the variation with distance from the nucleus of the density of molecules from which the modeled particles (H atoms in their case) collide is described by the strict density distribution of whole neutral water molecules expanding with a constant outflow speed and decaying due to photodestruction. Such a description is given by

$$N_{H_2O}(r) = \frac{Q}{4\pi v} \frac{1}{r^2} e^{-r/(v\tau)} \qquad (21)$$

where Q = the water production rate,

v = the outflow speed,

r = distance from the center of the nucleus,

τ = the photochemical lifetime of H_2O,

and N_{H_2O} = the number density of water.

Although this is correct for whole water molecules, this does not describe the radial dependence of collisional targets even for the case in question, i.e. a pure water coma with a constant outflow speed. As H_2O molecules are destroyed photochemically they produce various fragments, including H, and OH primarily but also H_2, O and various ions. All of these fragments also provide targets with which the modeled particle can collide. Since, to a very good approximation (Johnson 1986) the effective cross sectional area presented by a molecule for elastic collisions at low to moderate energies (~2 eV) is given approximately by the sum of the individual atomic cross sections, then ignoring the photodecay lifetime provides a better approximation to the radial dependence gas density as it applies to calculating collision path lengths. Furthermore, the absence of the exponential term, as we shall show shortly, provides an analytic solution for the probability density integral in the application of the Monte Carlo method for the case of hot H atom collisional thermalization.

Although we begin with the same formal application of the Monte Carlo method as Kitamura et al. (1985), the entire derivation will be presented here in the interest of completeness. The first step in this method is to calculate the collision path length for a single particle having a given location in the coma, and a given velocity vector direction. At least the first few

general steps also appear in the work of Cashwell and Everett (1959). Since the Monte Carlo method is inherently probabilistic, and we wish to derive an expression for the collision probability, we begin by considering a beam of n_0 particles traveling along a path with a linear coordinate, s, in a stationary medium with a number density, N(s), of scatterers each with a cross section of area, σ. If the beam of n_0 particles is displaced from s=0 to s=ds then by simple attenuation the number of particles scattered out of the beam, dn is given by,

$$dn = - n_0 N(0) \sigma \, ds.$$

In the case of a medium of uniform density, simple integration of this expression yields the exponentially decreasing attenuation law.

The case of interest here is that for a coma with a highly nonuniform density. For a nonuniform density this equation can be integrated (at least formally) to yield

$$\ln(n/n_0) = -\sigma \int_0^{s'} N(s'')ds'' \, . \tag{22}$$

This can alternatively be written

$$\frac{n}{n_0} = e^{-\sigma \int_0^{s'} N(s'')ds''} \, . \tag{23}$$

Returning to the Monte Carlo case of looking probabilistically at a single one of the n particles, Eq. 23 yields directly the probability for one particle to undergo a collision after traveling a distance, s', in the scattering medium to be

$$P(s') = 1 - e^{-\sigma_o \int^{s'} N(s'')ds''} \quad . \tag{24}$$

The probability density function for the collisional scattering process for use with the Monte Carlo principle (Eq. 1) then becomes

$$p(s')ds' = d(\sigma_o \int^{s'} N(s'')ds'')e^{-\sigma_o \int^{s'} N(s'')ds''} \quad . \tag{25}$$

Applying the Monte Carlo principle then yields the relation between a given random number and the path length for the collision of a single particle in a medium of arbitrary density to be,

$$1 - R_i = e^{-\sigma_o \int^{S} N(s')ds'} \quad , \tag{26}$$

which becomes

$$\sigma_o \int^{S} N(s')ds' = -\ln (1-R_i) \quad . \tag{27}$$

In the case of the cometary atmosphere, we shall assume (as discussed above) that the coma density is described as

$$N(r) = \frac{Q}{4\pi v} \frac{1}{r^2} \quad , \tag{28}$$

with r measured from the center of the cometary nucleus and, where the parameters are defined as in Eq. 21. We shall assume for this discussion that between collisions all the modeled particles (atoms or radicals) travel simple straight line trajectories. Even when radiation pressure acceleration is

important, the typical collision path lengths are much shorter than deviations of the true path from a straight line. Outside the very inner collision region, the radiation pressure accelerations are included in the trajectory calculations for relevant species. In situations where the radiation pressure is too large to ignore, the curved (parabolic) path can be divided into a set of straight line segments, each treated as discussed here.

The geometry relevant for the calculation of the collision length in a cometary atmosphere is illustrated in Figure 2. A particle is located at a distance r_o from the center of the nucleus and is moving in a direction such that its velocity vector makes an angle θ with the outward radial vector. At some arbitrary displacement along this path, ℓ', the density of molecules in the coma (Eq. 28) is given by

$$N[r(\ell')] = \frac{Q}{4\pi v} (r_o^2+\ell'^2+2r_o\ell'\cos\theta)^{-1} . \qquad (29)$$

However, since the particle is traveling through a radially outflowing coma, the path for collisions must be calculated relative to the moving coma gas and not in a (quasi-)stationary nucleus-centered frame. The exploded view in Figure 2 of the particle located at an arbitrary displacement ℓ' along the real path shows the appropriate projection geometry needed to calculate the apparent path through the moving gas. A real displacement $\Delta\ell$ along the real path can be separated into radial and tangential components, $(\Delta\ell)\cos\theta'$ and $(\Delta\ell)\sin\theta'$, respectively. If the particle is traveling at speed v_ℓ along the real path and the coma is flowing radially outward with a speed v, then, during the time the particle travels a distance $\Delta\ell$ along its path, the coma gas molecules move a distance $\Delta r = (v/v_\ell)\Delta\ell$ radially outward. The apparent path of the particle through the gas (Δs) is given by the vector sum of the

real tangential displacement and the relative radial displacement. This yields

$$\Delta s = \Delta \ell [1 - 2\beta \cos\theta' + \beta^2]^{1/2}, \tag{30}$$

where β is defined as the ratio of the radial outflow speed of the coma to the particle speed ($\beta = v/v_\ell$).

Since the coma density is a scalar function, it does not depend on the relative path between the particle and the coma, but only on the actual location in the coma. Therefore N(s) in Eq. 27 may be replaced functionally by $N[r(s(\ell'))] = N[r(\ell')]$ as given by Eq. 29. A change of variables in Eq. 27 from ds to $d\ell'$ may then be performed according to Eq. 30. Substituting Eq. 29 and the differential form of Eq. 30 into Eq. 27 and integrating along the apparent path in the rest frame of the nucleus yields the integral equation

$$-\ell n(1 - R_i) = \frac{\sigma Q}{4\pi} \int_o^\ell \frac{\left[1 - 2\beta\left(\frac{\ell' + r_o \cos\theta}{r_\ell'}\right) + \beta^2\right]^{1/2}}{v\, r_\ell'^{\,2}}\, d\ell' \tag{31}$$

where

$$r_\ell' = (r_o^2 + \ell'^2 + 2 r_o \ell' \cos\theta)^{1/2}.$$

There is no general analytical solution to this integral so that it can be solved for ℓ in the desired form, $\ell = \ell(R_i, \beta, \theta)$. However, it can be solved in certain limits or tabulated through numerical integration.

One important limit is that for a large particle speed ($\beta \to 0$), which is

important for the case of the collisional thermalization of hot H atoms. In fact, the original collision path calculation presented by Kitamura et al. (1985) is not the general case derived here (Eq. 31) but is only rigorously valid for β=0, and v = constant since they neglected the relative motions of the atoms and the coma gas molecules. By setting β to zero, Eq. 31 reduces to

$$-\ell n(1-R_i) = \frac{\sigma Q}{4\pi v} \int_0^{\ell} \frac{d\ell'}{\ell'^2+2r_o\ell'\cos\theta+r_o^2}$$

which can be integrated analytically and solved for ℓ for each collision of each particle. The result for a single collision path is

$$\ell = r_o \left\{ \sin\theta \tan\left[\frac{\pi}{2} - \theta - \left(\frac{4\pi v}{\sigma Q}\right) r_o \sin\theta \ln(1-R_i) \right] - \cos\theta \right\}. \quad (32)$$

For this case of spherical outflow at a constant speed, the group of parameters ($Q\sigma/4\pi v$) which occurs naturally in Eq. 31 is the traditional definition of the collision zone radius. It should also be pointed out that the argument of the tangent term (the term in [ ]) in Eq 32 is well defined physically only for values less than $\pi/2$. As the argument approaches $\pi/2$ from below, which happens more often for larger values of r_o, the collision path length approaches infinity, therefore values out of range imply complete escape of the particle.

For the case of spherical outflow with a variable speed as is implied by the results of gas-dynamic models (see section IV) the simple inverse square law in density does not exactly hold. In the most general situation Eqs. 28 and 29 must be modified in order to include a specified speed as a function of distance from the center of the nucleus, v(r). Then the integral in Eq. 31 would need to be solved numerically. However, the speed is a very slowly

changing variable in r as compared with any reasonable collision lengths, even in the outer coma where the collision paths are large as compared with the distance to the nucleus. Therefore, an excellent approximation can be made, which is to assume that the collision path is always given by the simple inverse square law referenced to the local value of the density. This is accomplished by replacing the speed, v, in Eqs. 28 and 32, by $v(r_o)$. This results in the following expression for the single Monte Carlo collision path length ℓ to be

$$\ell = r_o \left\{ \sin\theta \tan \left[\frac{\pi}{2} - \theta - \frac{\sin\theta \ln (1-R_i)}{r_o \sigma N(r_o)} \right] - \cos\theta \right\} .$$

A similar approximation can be made for the more general case, Eq. 31.

Once the particle is displaced this distance, ℓ, in the coma, it is scattered from an outflowing coma gas molecule. To this point we have assumed all collisions to be elastic and hard-sphere, where the mass of the molecule is the mean molecular mass of the coma gas. The coma at the given location, r_ℓ, can in general be considered to have a bulk outflow speed, $v(r_\ell)$, and a temperature, $T(r_\ell)$. The outflowing coma molecule is assigned a velocity in space, given as the vector sum of the radial outflow speed and a randomized thermal component. The random thermal speed component is given by Eqs. 18-20, whereas the random direction angles (in the radially outflowing frame of reference) are given by $\cos\theta_{th} = 1 - 2R_i$, and $\phi_{th} = 2\pi R_i$, again different random numbers are used for each angle. From the three-space velocity vectors of the modeled particle (radical or atom) and outflowing coma molecule, the straightforward mechanics of an elastic hard-sphere collision is performed. First, the center-of-mass of the collision between the given motion of the modeled particle and the thermal and radially outflowing molecule is found.

In an elastic collision, the exit velocity of the incoming modeled particle is isotropicized in the center-of-mass frame, given conservation of energy and momentum. The isotropization is done by computing two new random ejection directions in the center-of-mass frame and then transforming back to the coma (lab) frame. Also, the heating of the coma by each collision is calculated in radial intervals simply as the mechanical energy transfer per collision, which is given by

$$\Delta E = \frac{1}{2} m|\Delta\vec{v}|^2 \tag{33}$$

where $\Delta\vec{v}$ = change in velocity per collision in the coma (lab) frame, and m = mass of the modeled particle (radical or atom). After the new velocity vector is computed a new collision path can then be calculated. The modeled particle's trajectory is then followed until the the observation time, t_{obs}.

In the actual model computer code, modeled particles produced very deep in the collision zone ($r < 0.01\ R_c$ for H atoms, $r < 0.1\ R_c$ for heavy radicals, where $R_c = Q\sigma/4\pi v$), are assumed to be completely thermalized locally. They are then transported upward with the outflowing coma gas to the adopted boundary distance and re-released with an assumed random thermal plus outflow speed. Otherwise the particle could have to be followed for a very large number of collisions, which would be a needless waist of time. By choosing an optimal boundary the proper physics can be modeled in the most expedient manner.

Returning briefly to the expression for the collision path (Eq. 32), it is evident that there is both a directional (θ) as well as the radial dependence to the path length. Similarly to the case of a scattering medium with a uniform density, a mean free path can also be derived for the inverse square density dependence in the coma. The mean free path is defined such

that the abundance in a beam of particles travelling through a medium falls to 1/e of the original abundance. Then for Eq. 32, the mean free path is that value of ℓ such that $R_i = 1\text{-}e^{-1}$. In this case the mean free path has both a radial and a directional dependence. Figure 3 shows the loci of the mean free paths at a number of cometary distances relative to the collision zone radius R_c. Deep within the traditional collision zone the mean free path for collisions is not only small compared with the distance to the nucleus, it is also nearly independent of direction. When reaching distances of the order of the collision zone radius, the mean free path not only becomes much larger, it also becomes highly dependent on direction and favors radial escape.

In the case of hot H atoms, the large mass ratio between the H atoms and the generally heavy coma molecules causes the excess energy transfer per collision to be small and thus many collisions are required for the H atoms to thermalize completely. By inspection of Figure 3, then, one can see how the thermalization efficiency begins to fall from 100% at one-sixth to one-tenth of the collision radius, owing to the combination of the large mass ratio, large collision paths and favored radial escape.

III. Particle Trajectories in the Extended Coma

As discussed in section I of this paper, models of the large extended hydrogen cloud have been developed in order to explain the spatial morphology of the observed Lyman-α coma (Keller and Thomas 1975, Keller and Meier 1976). Festou et al. (1979) also applied the vectorial model (Festou 1981a,b) to analyze Lyman-α spectral line profiles of comet Bradfield. However, the models only addressed the inner coma, and were therefore (appropriately) steady-state, one-dimensional models which properly accounted for the isotropic ejection of H atoms upon photodissociation of OH and H_2O. On the other hand, the extended cloud models of Keller an co-workers included the effects of an isotropic point source of H atoms in which the outflow could be described by a Maxwell-Boltzmann speed distribution, solar radiation pressure, a variable production rate (typically of the form $Q=Q_0 r^{-n}$), and an ionization lifetime for the H atoms (of the form $\tau=\tau_0 r^2$). The effect of the different relative heliocentric orbits of the H atoms and the nucleus was accounted for by emitting the atoms from the syndyname as projected on the sky plane. Heliocentric distance and velocity dependent quantities were evaluated on the basis either of conditions at the location of the nucleus or on a column line-of-sight average.

Since the MCPTM method follows individual particles it is then possible to model even the three-dimensional, time-dependent extended distributions of coma atoms like H, C and O without the need of compromising approximations. Of course in some instances making approximations and reducing dimensionality does make the MCPTM more efficient (as is implicitly assumed in using other methods) however it is also possible to verify any approximations explicitly by considering a more general case. (This is difficult at best using other

methods.) A more detailed discussion of the advantages and numerical details appropriate to the H cloud model in particular and the resulting difference between the MCPTM and other modeling efforts are given in the companion paper (Paper 2).

The extended neutral cloud model uses the inner coma MCPTM described in the previous section for its source. It is therefore only necessary in this section to describe those parts of the extended MCPTM which pertain to the large scale geometry, sky plane projection and the orbital trajectory calculation. We have thus divided this section of the paper into two sections which deal with these areas. Some the numerical details have been placed in a separate Appendix in order to facilitate the flow of the derivations in this section.

Solution for the Heliocentric Trajectory of a Particle

The equation of motion for an atom or molecule in the coma may be readily reduced to a modified classical two-body problem of the form

$$\ddot{\vec{r}} = - \mu \frac{\vec{r}}{r^3} \tag{34}$$

where

$$\mu = GM - S \tag{35}$$

Here, G is the gravitational constant, M is the mass of the sun, and S/r^2 is the acceleration of solar radiation pressure on the gas atom or molecule. The simplest case occurs when S is a constant so that (34) reduces to the standard two-body equations. For hydrogen atoms, however, S is not a constant, but

depends upon the radial velocity of the atom relative to the sun because of the doppler shift out of the H Lyman- α absorption feature in the solar spectrum

$$S = S\left(\frac{\vec{r}\cdot\dot{\vec{r}}}{|\vec{r}|}\right) \tag{36}$$

Because of the dependence in Eq. 36 on the radial velocity of the atom, the equation of motion (34) is integrated numerically by adopting a fourth-order Runge-Kutta method and specifying appropriate initial conditions for the position and velocity of the atom. Equation (34) is solved in the heliocentric inertial frame $(\bar{x},\bar{y},\bar{z})$ discussed below (also see Appendix) and illustrated in Figure 4. Specification of the initial location $(\tilde{x}_0,\tilde{y}_0,\tilde{z}_0)$ and velocity $(\dot{\tilde{x}}_0,\dot{\tilde{y}}_0,\dot{\tilde{z}}_0)$ of the atom in the comet plane provides the required initial position $(\bar{x}_0,\bar{y}_0,\bar{z}_0)$ and velocity $(\dot{\bar{x}}_0,\dot{\bar{y}}_0,\dot{\bar{z}}_0)$ in the inertial frame

$$\begin{bmatrix} \bar{x}_0 \\ \bar{y}_0 \\ \bar{z}_0 \end{bmatrix} = \begin{bmatrix} \cos f & -\sin f & 0 \\ \sin f & \cos f & 0 \\ 0 & 0 & 1 \end{bmatrix} \begin{bmatrix} \tilde{x}+r_c \\ \tilde{y} \\ \tilde{z} \end{bmatrix} ,$$

and

$$\begin{bmatrix} \dot{\bar{x}}_0 \\ \dot{\bar{y}}_0 \\ \dot{\bar{z}}_0 \end{bmatrix} = \begin{bmatrix} \cos f & -\sin f & 0 \\ \sin f & \cos f & 0 \\ 0 & 0 & 1 \end{bmatrix} \begin{bmatrix} \dot{\tilde{x}}_0 + V_r - (\tilde{y}_0/r_e)v_f \\ \dot{\tilde{y}}_0 + ((\tilde{x}_0+r_c)/r_c)v_f \\ \dot{\tilde{z}}_0 \end{bmatrix}$$

that are needed to solve (34). In the above expressions, the location (r_c,f) and velocity (V_r,V_f) of the comet at the time of the initial conditions are determined by a method to be described below.

Geometry for the Comet and the Cometary Atmosphere

To describe the spatial morphology of gas atoms and molecules in the comet atmosphere, a geometric mapping that relates the location of an atom or molecule in an inertial sun-centered coordinate frame $(\bar{x},\bar{y},\bar{z})$ to its apparent position in the earth sky-plane (M',N'), centered on the comet, is required. In Figure 4, the comet location, comet orbit plane, and comet orbit are illustrated relative to the Earth and Sun. Also depicted in Figure 4 are the inertial frame $(\bar{x},\bar{y},\bar{z})$ and two comet centered coordinate frames: the Sun-oriented $(\tilde{x},\tilde{y},\tilde{z})$ coordinate frame and the historically adopted (see Finson and Probstein, 1968) Earth-orientated (L,M,N) coordinate frame. Including parallax projection, the Earth sky-plane coordinates (M',N') for an atom or molecule at location (L_o,M_o,N_o) in the (L,M,N) coordinate system are defined by the parallax projection on the (M,N) plane, and are given by

$$M' = M_0\left(1 + \frac{L_o}{\rho_c - L_o}\right) \tag{37a}$$

$$N' = N_0\left(1 + \frac{L_o}{\rho_c - L_o}\right) \tag{37b}$$

where ρ_c is the distance of the comet from the Earth.

The Sun-centered inertial coordinate frame $(\bar{x},\bar{y},\bar{z})$ is defined with the $\bar{z}$-axis normal to the comet orbit plane, and with the $\bar{x}$-axis directed from the Sun through the perihelion point of the comet orbit located a distance q from the center of the Sun. The trajectories of atoms or molecules escaping the comet may be calculated in this coordinate frame by methods described already. The comet location in the $(\bar{x},\bar{y})$ plane is determined by the angle f between the $\bar{x}$-axis and the Sun-comet direction, and by the sun-comet distance r_c. The quantities r_c and f, which depend upon the comet orbit eccentricity e and perihelion distance q as well as the difference between the absolute observation time t and the perihelion passage time τ, are calculated by methods to be described later. The $(\tilde{x},\tilde{y},\tilde{z})$ comet centered coordinate frame is defined so that the ($\tilde{z}$-axis) is normal to the comet plane, and the positive $\tilde{x}$-axis is along the Sun-comet direction so that the Sun is located at $(-r_c,0,0)$. A point in the inertial frame $(\bar{x},\bar{y},\bar{z})$ is therefore transformed to the $(\tilde{x},\tilde{y},\tilde{z})$ frame by a simple rotation about the $\bar{z}$-axis followed by a simple translation along the sun-comet direction:

$$\begin{pmatrix} \tilde{x}+r_c \\ \tilde{y} \\ \tilde{z} \end{pmatrix} = \begin{pmatrix} \cos f & \sin f & 0 \\ -\sin f & \cos f & 0 \\ 0 & 0 & 1 \end{pmatrix} \begin{pmatrix} \bar{x} \\ \bar{y} \\ \bar{z} \end{pmatrix} \qquad (38)$$

The (L,M,N) coordinate frame is defined with the positive L-axis along the comet-Earth direction, the positive M-axis perpendicular to the L-axis and in the plane formed by the Sun-comet and Sun-Earth lines, and the N-axis normal to the (L,M) plane as shown in Figure 4. The transformation between the (L,M,N) frame and the $(\tilde{x},\tilde{y},\tilde{z})$ frame is given by (see Finson and Probestein, 1968)

$$\begin{bmatrix} L \\ M \\ N \end{bmatrix} - \begin{bmatrix} \frac{\tilde{x}_E}{\rho_c} & \frac{\tilde{y}_E}{\rho_c} & \frac{\tilde{z}_E}{\rho_c} \\ \frac{(\tilde{y}_E^2+\tilde{z}_E^2)^{1/2}}{\rho_c} & \frac{-\tilde{x}_E\tilde{y}_E}{\rho_c(\tilde{y}_E^2+\tilde{z}_E^2)^{1/2}} & \frac{-\tilde{x}_E\tilde{z}_E}{\rho_c(\tilde{y}_E^2+\tilde{z}_E^2)^{1/2}} \\ 0 & \frac{\tilde{z}_E}{(\tilde{y}_E^2+\tilde{z}_E^2)^{1/2}} & \frac{-\tilde{y}_E}{(\tilde{y}_E^2+\tilde{z}_E^2)^{1/2}} \end{bmatrix} \begin{bmatrix} \tilde{x} \\ \tilde{y} \\ \tilde{z} \end{bmatrix} \tag{39}$$

where

$$\rho_c = (\tilde{x}_E^2+\tilde{y}_E^2+\tilde{z}_E^2)^{1/2} \ .$$

Here $(\tilde{x}_E,\tilde{y}_E,\tilde{z}_E)$ are the coordinates of the Earth in the $(\tilde{x},\tilde{y},\tilde{z})$ frame given by

$$\begin{pmatrix} X_E+r_c \\ Y_E \\ Z_E \end{pmatrix} = - \begin{pmatrix} l_{\tilde{x}} & m_{\tilde{x}} & n_{\tilde{x}} \\ l_{\tilde{y}} & m_{\tilde{y}} & n_{\tilde{y}} \\ l_{\tilde{z}} & m_{\tilde{z}} & n_{\tilde{z}} \end{pmatrix} \begin{pmatrix} X \\ Y \\ Z \end{pmatrix} \tag{40}$$

where the unit vectors $(l_{\bar{x}},m_{\bar{x}},n_{\bar{x}})$, $(l_{\bar{y}},m_{\bar{y}},n_{\bar{y}})$ and $(l_{\bar{z}},m_{\bar{z}},n_{\bar{z}})$ are defined in the Appendix and where (X,Y,Z) are the geocentric equatorial rectangular coordinates of the Sun (see the Appendix). To determine the transformation (40), the six orbital elements of the comet (w,Ω,i,q,e,T), the obliquity ϵ of the Earth, and the absolute time t at which the comet is observed must also be specified. For a particular atom or molecule location $(\bar{x}_p,\bar{y}_p,\bar{z}_p)$ in the $(\bar{x},\bar{y},\bar{z})$ inertial coordinate frame, the desired Earth sky-plane coordinates of the particle (M'_p,N'_p) may therefore be determined by using Eqs. 38 and 39 in Eq. 37 and may be symbolically denoted by

$$M'_p = M'_p\ (\bar{x}_p,\bar{y}_p,\bar{z}_p|w,\Omega,i,q,e,\tau|X,Y,Z,\epsilon|t) \tag{41a}$$

$$N'_p = N'_p\ (\bar{x}_p,\bar{y}_p,\bar{z}_p|w,\Omega,i,q,e,\tau|X,Y,Z,\epsilon|t)\ . \tag{41b}$$

The equation of motion for a comet in the gravitational field of the Sun is readily reduced to the classical two-body problem and exhibits orbits that are conic sections with the sun at a focus. The conic section in polar coordinates (r,f) (see Figure 4),

$$r = \frac{p}{1+e\ \cos\ f}\ ,$$

and its exact shape are completely determined by the eccentricity e (e<1 ellipse; e=1 parabola; e>1 hyperbola) and the perihelion distance q (P=q(1+e) ellipse; P=2q parabola; P=q(1-e) hyperbola). The position and velocity of the comet on its conic section orbit at a given time t depend upon the lapse time $t-\tau$ between that time and the perihelion passage time τ. By integrating the equations of motion, an expression for $t-\tau$ involving transcendental functions of f can always be determined, but the inversion of the expression to determine f as a function of $t-\tau$ (with the exception of the parabolic orbit) is not algebraically tractable. This requires that the expression for $t-\tau$ be inverted numerically by using a simple iterative scheme. For an elliptic orbit with an eccentricity in the range $0 \leq e < 0.95$ and for a hyperbolic orbit with an eccentricity $e > 1.05$, standard iterative methods (see Roy, 1965) are employed to determine the polar coordinate position (r,f) and velocity (v_r, v_f) of the comet at a lapse time $t-\tau$. For values of the eccentricity in the range $0.95 \leq e < 1.05$, the Gauss method (see Benima, Chernizak, and Marsden, 1969) is definitely a superior numerical method and has been adopted here.

IV. Photochemical Heating

Deep within the collision zone mean free paths for intermolecular collisions are very small compared with the distance to the nucleus and thus are small compared with changes in density (due mainly to the dominant $1/r^2$ distribution). In the transition region the mean free path is however highly dependent on direction and favors radial escape, as discussed in section 2 (see also Figure 3). This effect is especially important for the case of collisional thermalization of cometary hydrogen which is produced with an excess kinetic energy of ~2.6 eV during the photodissociation of water. Because of the large mass ratio between the heavy parent gas (~18 amu) and H atoms (1 amu) only 10% of the excess energy possessed by the H atom is transferred to the parent gas per collision. Therefore it takes many collisions for an H atom to thermalize completely. For example it takes 7 collisions to lose 50% its energy, and 22 collisions to lose 90% of its energy. With the directional dependence of the mean free path in mind it becomes clear that many H atoms produced well inside the collision zone will eventually escape without being completely thermalized. Ip (1983) and Crovisier (1984) have recognized this fact and have pointed out that the only way of effectively calculating this effect is through a multiple collisional Monte Carlo model. The effect of the collisional decoupling is important not only for determining the photochemical heating rate in the coma but also for determining the outflow speed distribution of H atoms from the inner coma which shapes the observed morphology of the Lyman-α coma (Paper 2).

Both Ip (1983) and Crovisier (1984) have demonstrated that the essential physical development (i.e., the radial dependence of gas temperature and outflow speed) of a water dominated cometary coma can be reasonably estimated

by considering a simple gas-dynamic model of a pure water coma where the only heating mechanism is the thermalization of hot H atoms produced by the photodissociation of water molecules. In fact, Bockelee-Morvan and Crovisier (1987) find that both the gas temperature, as inferred by the near IR observation of H_2O in comet Halley, and the outflow speeds determined from the doppler widths of rotational lines of HCN, as measured in radio observations of comet Halley agree rather well with the prediction of such a simple model. In order to calculate the effect of collisional decoupling of H atoms from the coma, a procedure has been developed to iterate between the steady state inner coma MCPTM which explicitly calculates the correct heating rate and a gas-dynamic model which calculates the outflow speed and temperature. Since the approximate $1/r^2$ density distribution dominates the collision rate, convergence is quite rapid.

A discussion of the basic procedure as well as the first results of its use have already been briefly presented by Combi (1987). We have adopted a multi-species single-fluid gas-dynamic model for the physical development of the cometary coma. The model is based on the equations of mass, momentum and energy conservation and the ideal gas law, which are given as

$$\rho = Qm/4\pi v r^2, \tag{42}$$

$$\rho v \frac{dv}{dr} = - \frac{dP}{dr}, \tag{43}$$

$$\frac{1}{r^2} \frac{d}{dr} \left[\rho v r^2 \left(\frac{v^2}{2} + \frac{\gamma}{\gamma-1} \frac{P}{\rho} \right) \right] = S - L, \tag{44}$$

$$P = \frac{\rho k T}{m} \tag{45}$$

where ρ = mass density, Q = gas production rate in molecules per second, m = mean molecular mass, v = bulk outflow speed, P = pressure, T = gas temperature, γ = ratio of the specific heats, and S and L are the heating and cooling rates. The appropriate quantities, namely m and γ are species averaged (Huebner and Keady 1983), and the detailed water photochemistry (see Paper 2) is followed. It has been demonstrated that the gas-dust interaction in the very inner coma may be quite important. Original dusty gas models (Marconi and Mendis 1984; Gombosi et al, 1985) found that the main effect of dust on the gas dynamics was a mass loading which slowed the gas outflow so that inner coma speeds only reached values of ~0.65 km/s. More recent work suggests the possibility that there is a strong infrared radiation coupling between the water-dominated gas and the dust (Marconi and Mendis 1986). This results in higher outflow speeds of ~1 km/s and higher gas temperatures of ~200 K at 100 km from the nucleus.

However, in recent work by Bockelee-Morvan and Crovisier (1987), in which they approximated the collisional decoupling of hot H atoms, they have found that a simple gas-dynamic model (with a photochemical heating efficiency less than unity) can explain the general levels of both the cool temperatures inferred from IR spectra of water, as well as the outflow speeds inferred from the doppler widths of HCN radio lines observed in comet Halley. From this they conclude that the infrared radiation coupling of gas and dust suggested by Marconi and Mendis (1986) is not important and can be neglected. Furthermore, the agreement of our modeled Lyman-α isophotes of comet Kohoutek (in Paper 2) using only a simple gas-dynamic model also supports this contention.

We begin with the velocity and temperature from a simple pure gas-dynamic model. This temperature and velocity field is used as the input to

characterize the distribution of the outflowing coma gases, as they serve as both the extended source for the H atoms and as the collisional scattering background for the trajectories of the H atoms. The steady-state inner coma MCPTM is then used to calculate the new heating rate explicitly by counting the energy deposited in each collision by every H atom. This heating rate as a function of radial distance is then used for the term, S in the gas-dynamic model (Eq 44). The resulting temperature and velocity fields from the modified gas-dynamic model are then used again in the inner coma MCPTM, and the process is iterated until a convergent solution is reached.

Unlike the original Monte Carlo models (Combi and Delsemme 1980a) the coma includes the effects of the variable outflow speed and the temperature on the initial space-velocity distribution of the H atoms. The parent dissociation time is calculated according to Eq. 2 but now the radial positions of the parents are calculated not assuming a constant speed but using the radial postion as a function of time, which is generated in the gas-dynamic model. A daughter H atom is then emitted from the center-of-mass motion of the parent water molecule, which has a radial component and a random thermal component from the local gas temperature, with an excess speed determined from the excess photodissociation energy spectrum. The details of the water (and OH) photochemistry are given in Paper 2.

The results of a sample calculation of this type are shown in Figure 5. The results of the coupled gas-dynamic/MCPTM calculation (lower heavy lines) are compared with a simple gas-dynamic model (upper thin lines) for the case of a 100% water coma at 1 AU from the sun and a production rate of 10^{29} molecules per second. The pure gas-dynamic results were obtained using the standard constant heating rate as in the results of Ip (1983) and Crovisier (1984). For both sets of calculations the results are cut off at the

collision radius since the gas-dynamic model is no longer appropriate at these distances.

The importance of the collisional decoupling of H atoms is most evident in the comparison of the heating rates in the two calculations. The H atoms begin to decouple fully one order of magnitude inside the traditional collision zone, and the rate decreases a little faster than 1/r thereafter. This is in contrast to Ip's (1983) estimate of the decoupling which falls exponentially since it takes into account the lack of local thermalization of locally produced H atoms, but does not account for the collisional heating from non-locally produced H atoms. A less severe, exponential form has also been suggested by Kitamura (1986).

The effect of the hot H atom collisional decoupling is best demonstrated in Figure 3 which shows the directional and radial dependence of the mean free path. We thus find outer coma temperatures which are substantially lower (30K) than those predicted by simple gas-dynamic models (120K) at the collision radius (~3000 km). The outflow speed is only slightly modified in this case, however for comets with a higher gas production (and larger collision zone) differences in speed also become substantial (Combi 1987).

As mentioned the inner coma MCPTM includes the radial dependence for both the gas temperature and outflow speed, so the coma gas is considered to have a variable convected Maxwellian speed distribution. This is an important improvement over the model of Kitamura et al. (1985) which considered the coma to have a constant outflow speed and essentially a zero temperature. This importance is twofold. First, the heating (collision) rate is coupled in a non-linear fashion to the outflow speed and thus is somewhat self regulating (through the coupled fluid equations). Second, the exit speed distribution of the more thermalized H atoms is a superpostion of the bulk gas outflow speed

and a (partially) thermalized speed which is substantial for light H atoms even at these low temperatures (ten to several hundred Kelvin). This is very important for shaping the morphology of the extended hydrogen coma, which is a sensitive indicator of the effective outflow speed distribution of H atoms exiting the inner collisional coma. An extensive discussion of our early attempts to model observed isophobes of the Lyman-α coma of comet Kahoutek (Paper 2) demonstrates that the specification of physically realistic conditions (coma temperature and outflow speed) is required in order to obtain good model-data agreement.

The gas-dynamic model results presented by Bockelee-Morvan and Crovisier (1987) are based on a single Monte Carlo simulation for the collisional decoupling of H atoms from the heavy outflowing (mainly H_2O) gas. They have adopted the analytical approximation of Kitamura (1986) to describe the results of a single explicit Monte Carlo simulation, and apparently extrapolate the analytical form to a variety of cases. They do not explicitly include the Monte Carlo calculation in the iterative procedure as we do here and as was presented in earlier results (Combi 1987). They, on the other hand, explicitly iterate the IR raditive transfer effect in the inner coma cooling rate whereas we adopt the approximation of Huebner and Keady (1983) for IR trapping. One objection to the analytic form suggested by Kitamura (1986) is that the photochemical heating efficiency falls exponentially outside some critical radius as did that assumed by Ip (1983) although the drop-off is actually not as severe. Through a number of Monte Carlo simulations we find, however, that heating efficiency begins to depart from complete thermalization much closer to the nucleus than Kitamura's expression but then only falls with an inverse power law in the distance to the nucleus having an exponent slightly more negative than -1.

V. Summary

In this paper we have presented the mathematical descriptions for the methods employed in our general Monte Carlo particle trajectory model (MCPTM). These methods allow for the proper treatment to be made for many physical processes which are important in both the outer extended atom comae, and the inner radical comae of comets. Some of the new methods introduced here have been developed in the interest of computational efficiency, while others are the inclusion of new physical processes or dimensional generalizations. The application of the MCPTM to the spatially extended, time-dependent, and three-dimensional Lyman-α coma is the subject of the accompanying paper in this volume (Combi and Smyth 1987b, Paper 2). One application which is presented in this paper is the proper calculation of the photochemical heating of the cometary coma due to the collisions of hot H atoms produced in the photo-dissociation of water molecules with the coma gases. In order to study this problem the coupled gas-dynamic/MCPTM introduced by Combi (1987) has been discussed in detail here. We find that the collisional decoupling of the hot H atoms from the heavy parent coma gas well inside the traditionally defined collision zone causes the appropriately modeled coma to have lower outflow speeds and substantially lower temperatures. Previous attempts to approximate analytical solutions to this decoupling have resulted in the incorrect functional form and/or a gross overestimation of the decoupling.

The methods presented in this paper will be used in future work to study the effects on the spatial distributions of observed chemical species (radicals and atoms) and to explore the basic physics of the transition zone between true fluid-flow to free molecular flow. In our preliminary work, we find that the transition zone is large and limits the spatial extent to which purely collisional fluid models can be applied. Furthermore, in large, bright

comets like Halley, typical ground-based observations covered the spatial domain of the transition zone itself. Whereas for smaller comets, where observations are typically made outside the transition zone, the true initial conditions for appropriate free molecular flow (exospheric) models are in fact still determined by conditions in the inner and transition regions.

Acknowledgments

Support for this research was provided by contracts NASW-3950 and NASW-3966 from the Planetary Atmospheres program at NASA. We would like to thank Drs. Bockelee-Morvan and Crovisier for communicating their work to us prior to publication, and Dr. R. Johnson for helpful discussions regarding molecular scattering. The careful and patent reading of this paper by an anonymous referee, and the constructive comments are gratefully acknowledged.

References

Benima, B., Cherniack, J.R., Marsden, B.G. and Porter, J.G., 1969, PASP, 81, 121.

Bockelee-Morvan, D. and Crovisier, J., 1987, Proc. of the Symposium on the Diversity and Similarity of Comets, Brussels, Belgium, (in press).

Bockelée-Morvan, D. and Gerard, E., 1984, Astr. Ap., 131, 111.

Cashwell, E.D. and Everett, C.J., 1959, "The Monte Carlo Method for Random Walk Problems," Pergamon Press, p.28.

Chamberlain, J.W., 1963, Plant. Space Sci., 11, 901.

Cochran, A.L., 1985, Icarus, 62, 82.

Combi, M.R., 1980, Ap. J., 241, 830.

Combi, M.R., 1987, Icarus, 71, 178.

Combi, M.R. and Delsemme, A.H., 1980a, Ap. J., 237, 633.

Combi, M.R. and Delsemme, A.H., 1980b, Ap. J., 237, 641.

Combi, M.R. and Smyth, W.H., 1985, Bull. Amer. Astron. Soc., 17, 724.

Combi, M.R. and Smyth, W.H., 1987a, Symposium on the Diversity and Similarity of Comets, Brussels, Belgium, 6-9 April 1987.

Combi, M.R. and Smyth, W.H., 1987b, Ap. J., (Paper 2).

Combi, M.R., Stewart, A.I.F. and Smyth, W.H., 1986. GRL, 13, 385.

Crovisier, J., 1984, Astr. Ap., 130, 361.

Eddington, A.S., 1910, M. N. R. A. S., 79, 442.

Fahr, H.J. and Shizgal, B, 1983, Rev. of Geophys. and Sp. Sci., 21, 75.

Festou, M.C., 1981a, Astr. Ap., 95, 69.

Festou, M.C., 1981b, Astr. Ap., 96, 52.

Festou, M., Jenkins, G.B., Keller, H.U., Barker, E.S., Bertaux, J.L., Drake, J.F. and Upson, W.L., 1979, Ap. J., 223, 638.

Finson, M.L. and Probstein, R.F., 1968, Ap. J. 154, 327.

Giguere, P.T. and Huebner, W.F., 1978, Ap. J., 223, 638.

Gombosi, T.I., Cravens, T.E. and Nagy, A.F., 1985, Ap. J., 293, 328.

Gombosi, T.I., Nagy A.F., and Cravens, T.E., 1986, Rev. Geophys. 24, 667.

Haser, L., 1957, Bull. Acad. Roy. Soc. Belgique, 43, 740.

Haser, L., 1966, Mem. Soc. Roy. Sci. Liege, 12, series 5, 233.

Huebner, W.F. and Keady, J.J., 1983, International Conference on Cometary Exploration, Hungarian Academy of Sciences.

Ip, W.-H., 1983, Ap. J., 264, 726.

Keller, H.U. and Meier, R.R., 1976, Astr. Ap., 52, 273.

Keller, H.U. and Thomas, G.E., 1975, Astr. Ap., 39, 7.

Kitamura, Y., 1986, Icarus, 66, 241.

Kitamura, Y., Ashihara, O. and Yamamota, T., 1985, Icarus, 61, 278.

Kömle, N.I. and Ip, W.-H., 1986, Exploration of Halley's Comet, ESA-SP-250, 86.

Marconi, M.L. and Mendis, D.A., 1982, Ap. J., 260, 386.

Marconi, M.L. and Mendis, D.A., 1983. Ap. J., 273, 381.

Marconi, M.L. and Mendis, D.A., 1984, Ap. J., 287, 445.

Marconi, M.L. and Mendis, D.A., 1986, The Moon and Planets, 36, 249.

Meier, R.R., Opal, C.B., Keller, H.U., Page, T.L., Caruthers, G.R., 1976, Astr. Ap., 52, 283.

Mendis, P.A. and Ip, W.-H., 1975, Ap. & Sp. Sci., 39, 335.

Mitchell, G.F., Prasad, S.S. and Huntress, W.T., 1981, Ap. J., 244, 1087.

Roy, A.E., 1965, The Foundations of Astrodynamics, the Macmillan Co., New York.

Schloerb, F.P. and Gerard, E., 1985, A. J., 90, 1117.

Wallace, L.V. and Miller, F.D., 1958, A. J., 63, 213.

Appendix

The coordinates $(\tilde{x}_E, \tilde{y}_E, \tilde{z}_E)$ of the Earth in the comet centered coordinate frame $(\tilde{x}, \tilde{y}, \tilde{z})$ were defined in the text by the transformation

$$\begin{pmatrix} \tilde{x}_E + r_c \\ \tilde{y}_E \\ \tilde{z}_E \end{pmatrix} = - \begin{pmatrix} l_{\tilde{x}} & m_{\tilde{x}} & n_{\tilde{x}} \\ l_{\tilde{y}} & m_{\tilde{y}} & n_{\tilde{y}} \\ l_{\tilde{z}} & m_{\tilde{z}} & n_{\tilde{z}} \end{pmatrix} \begin{pmatrix} X \\ Y \\ Z \end{pmatrix} \tag{A.1}$$

where (X,Y,Z) are the geocentric equatorial rectangular coordinates of the Sun or alternatively (-X,-Y,-Z) are the heliocentric rectangular coordinates of the Earth. The three rows of the transformation matrix in (A.1) are, respectively, the three unit vectors of the direction of the $\tilde{x}$-axis, $\tilde{y}$-axis and $\tilde{z}$-axis in the geocentric equatorial coordinate system:

$$i_{\tilde{x}} = (l_{\tilde{x}}, m_{\tilde{x}}, n_{\tilde{x}}) \tag{A.2.a}$$

$$i_{\tilde{y}} = (l_{\tilde{y}}, m_{\tilde{y}}, n_{\tilde{y}}) \tag{A.2.b}$$

$$i_{\tilde{z}} = (l_{\tilde{z}}, m_{\tilde{z}}, n_{\tilde{z}}) \tag{A.2.c}$$

The geocentric equatorial coordinate system $(\bar{x}, \bar{y}, \bar{z})$ has its $\bar{x}$-axis along the vernal equinox direction (γ) and its $\bar{z}$-axis normal to the equator plane. The relative orientation of the equator plane, the ecliptic plane, and the comet plane are illustrated in Figure A.1. Also depicted in Figure A.1 are the obliquity of the ecliptic ϵ, the comet plane elements (Ω, ω, i), the sun-

centered inertial frame $(\bar{\bar{x}},\bar{\bar{y}},\bar{\bar{z}})$, the comet's polar coordinates (r_c,f) in the $(\bar{\bar{x}},\bar{\bar{y}})$ frame, and the comet centered coordinate frame $(\tilde{x},\tilde{y},\tilde{z})$.

The elements of the unit vectors in (A.2) follow from Figure 2 and are given by

$$l_{\tilde{x}} = \cos(\omega+f)\cos\Omega - \sin(\omega+f)\sin\Omega\cos i \tag{A.3.a}$$

$$l_{\tilde{y}} = -\sin(\omega+f)\cos\Omega - \cos(\omega+f)\sin\Omega\cos i \tag{A.3.b}$$

$$l_{\tilde{z}} = \sin i \sin\Omega \tag{A.3.c}$$

$$m_{\tilde{x}} = [\cos(\omega+f)\sin\Omega + \sin(\omega+f)\cos\Omega\cos i]\cos\epsilon - \sin(\omega+f)\sin i\sin\epsilon \tag{A.4.a}$$

$$m_{\tilde{y}} = [-\sin(\omega+f)\sin\Omega + \cos(\omega+f)\cos\Omega\cos i]\cos\epsilon - \cos(\omega+f)\sin i\sin\epsilon \tag{A.4.b}$$

$$m_{\tilde{z}} = -\sin i\cos\Omega\cos\epsilon - \cos i\sin\epsilon \tag{A.4.c}$$

$$n_{\tilde{x}} = [\cos(\omega+f)\sin\Omega + \sin(\omega+f)\cos\Omega\cos i]\sin\epsilon + \sin(\omega+f)\sin i\cos\epsilon \tag{A.5.a}$$

$$n_{\tilde{y}} = [-\sin(\omega+f)\sin\Omega + \cos(\omega+f)\cos\Omega\cos i]\sin\epsilon + \cos(\omega+f)\sin i\cos\epsilon \tag{A.5.b}$$

$$n_{\tilde{z}} = -\sin i\cos\Omega\sin\epsilon + \cos i\cos\epsilon \tag{A.5.c}$$

Michael R. Combi and William H. Smyth

Atmospheric and Environmental Research, Inc.

840 Memorial Drive

Cambridge, MA 02139-3758

52, 53

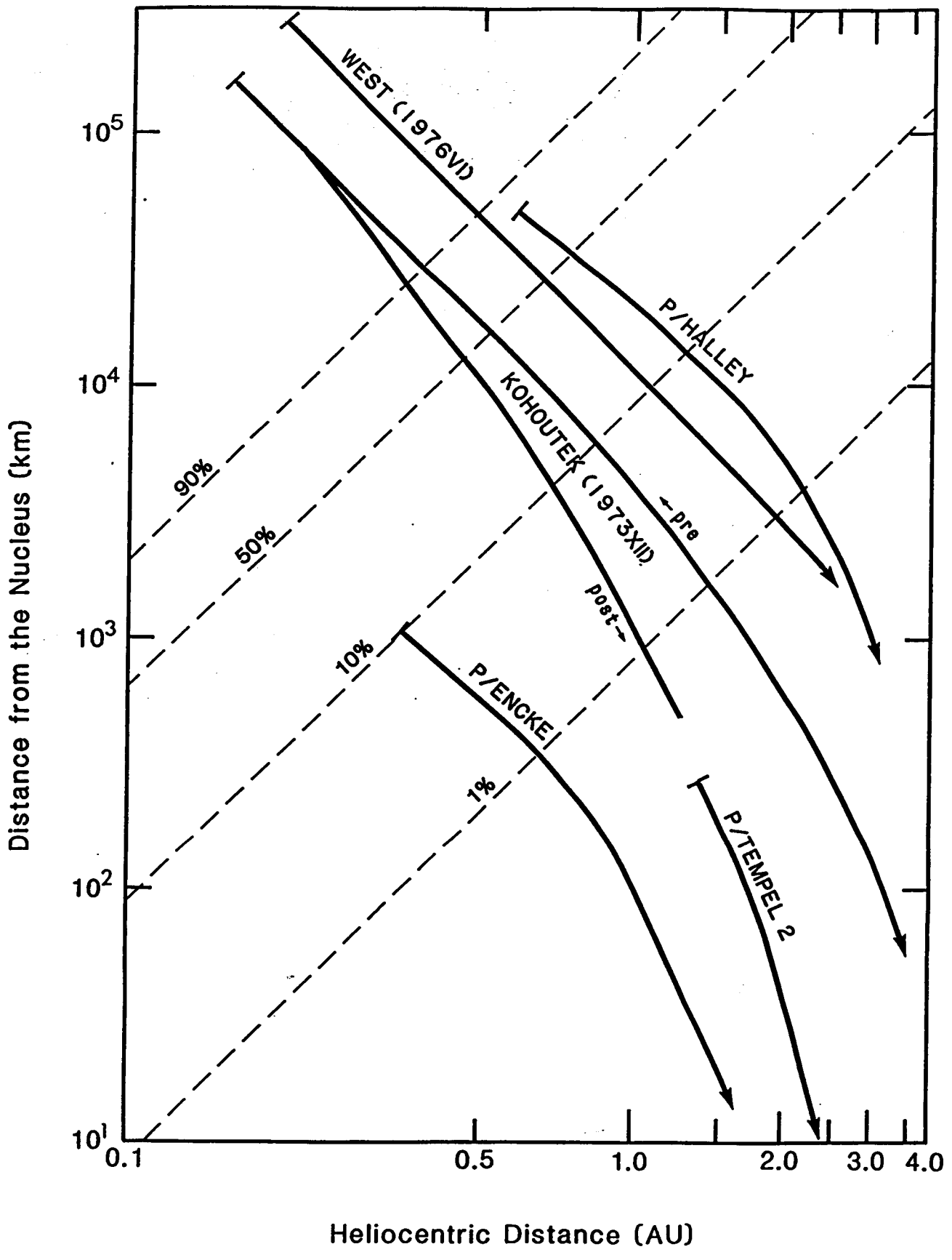
WEST (1976VI)
P/HALLEY
KOHOUTEK (1973XII)
pre
post
P/ENCKE
P/TEMPEL 2
90%
50%
10%
1%
10^5
10^4
10^3
10^2
10^1
0.1
0.5
1.0
2.0
3.0
4.0
Distance from the Nucleus (km)
Heliocentric Distance (AU)

FIGURE 1

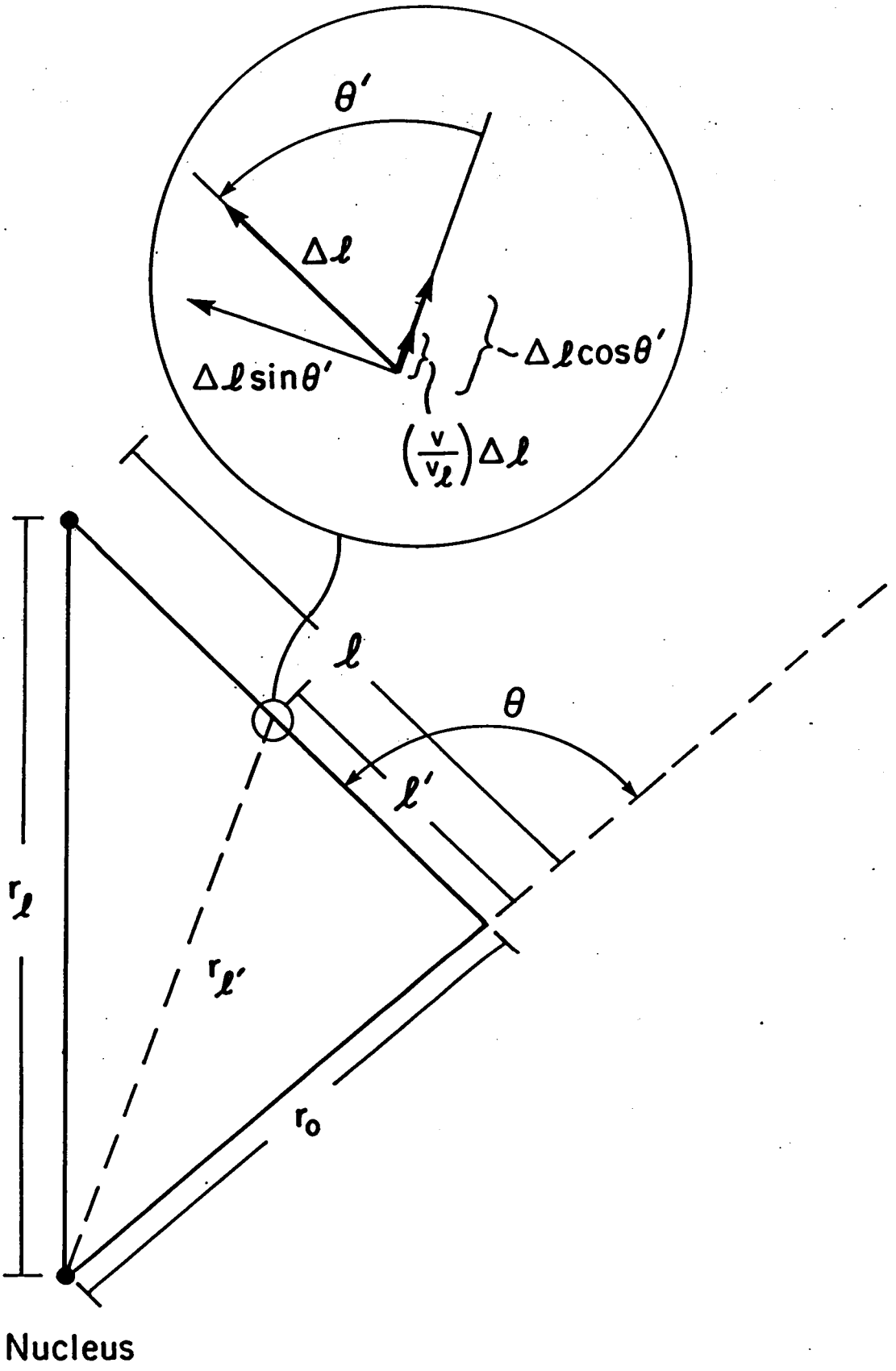

FIGURE 2

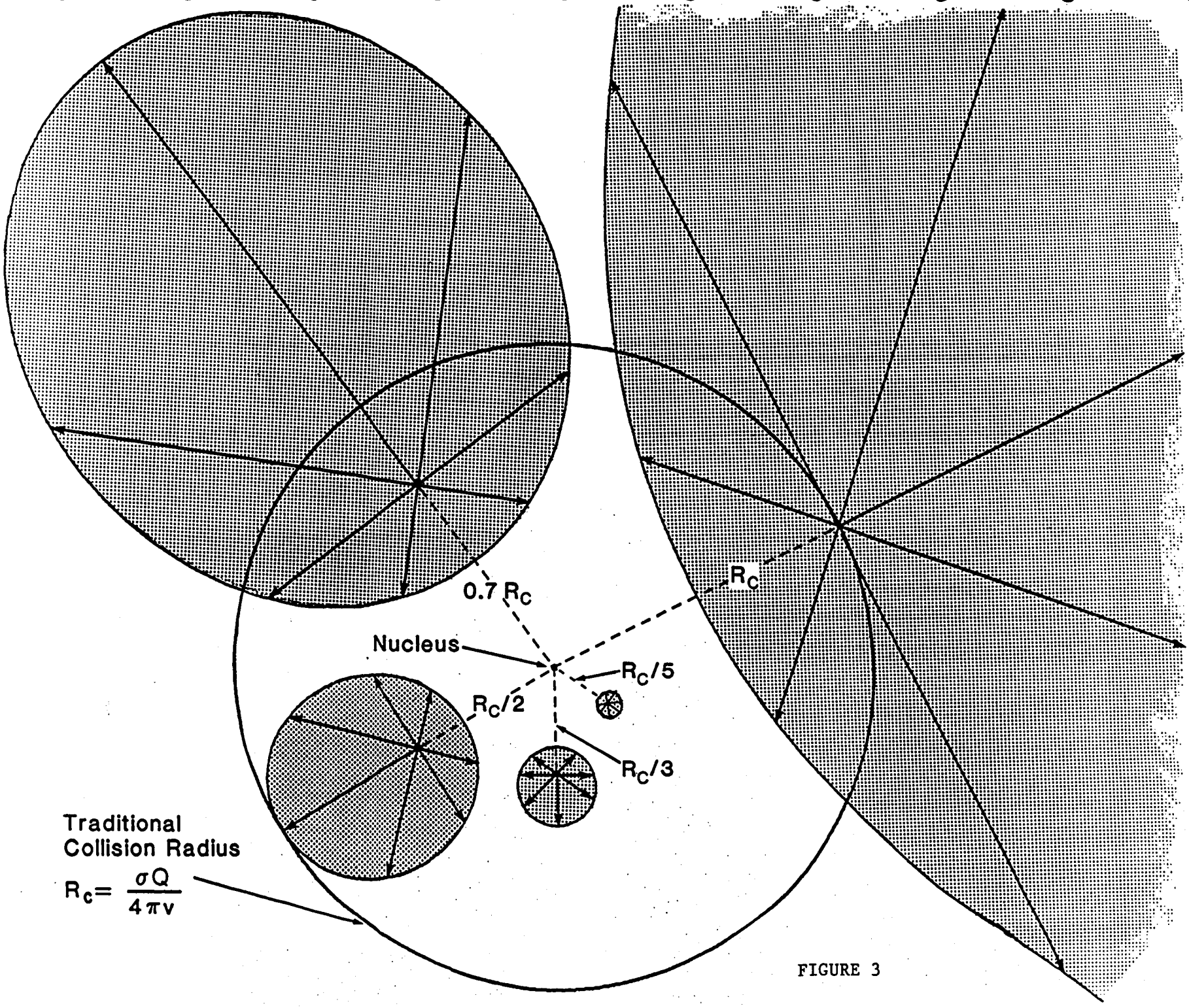
0.7 Rc
Rc
Nucleus
Rc/5
Rc/2
Rc/3
Traditional
Collision Radius
Rc= σQ / 4πv

FIGURE 3

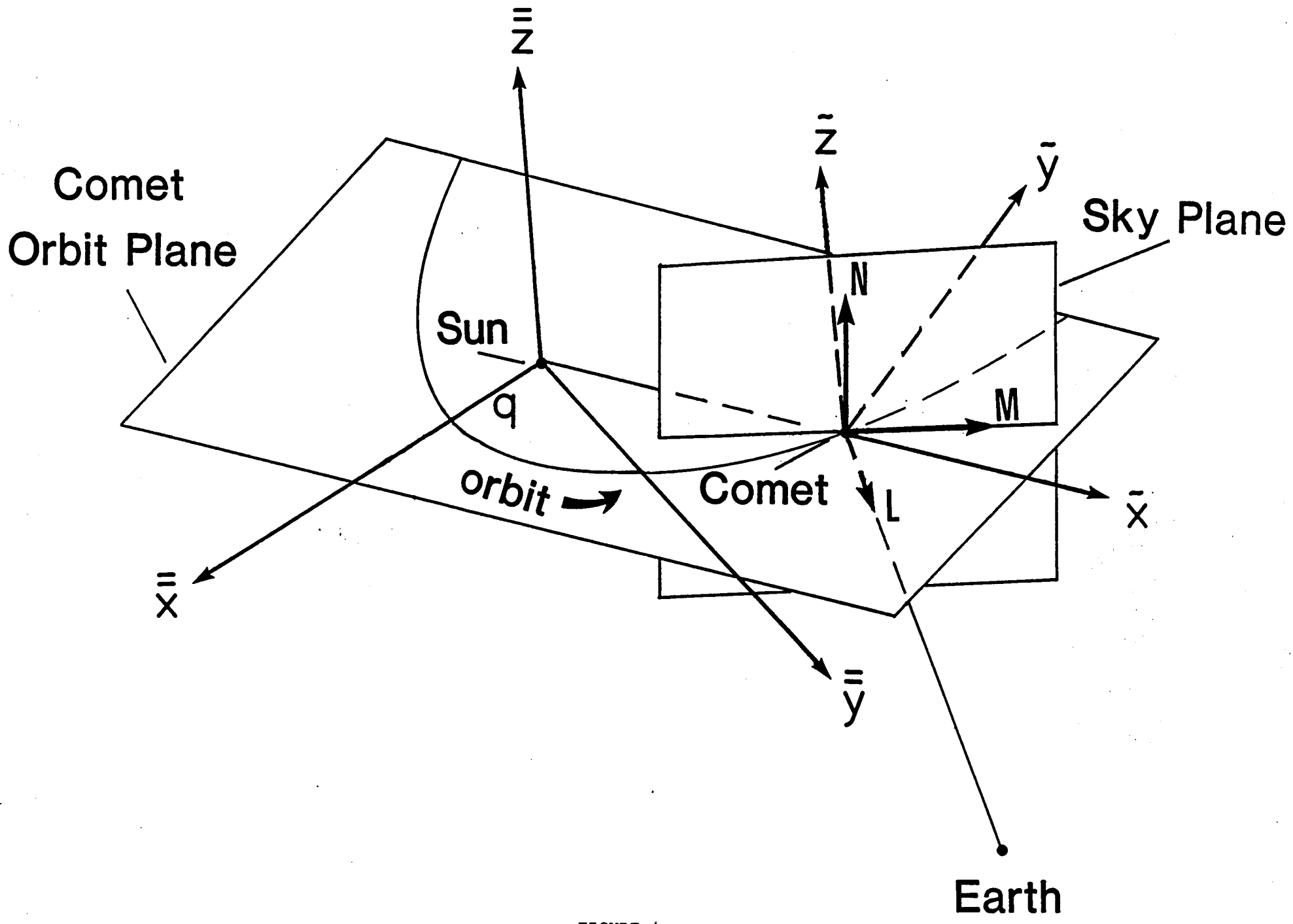

FIGURE 4

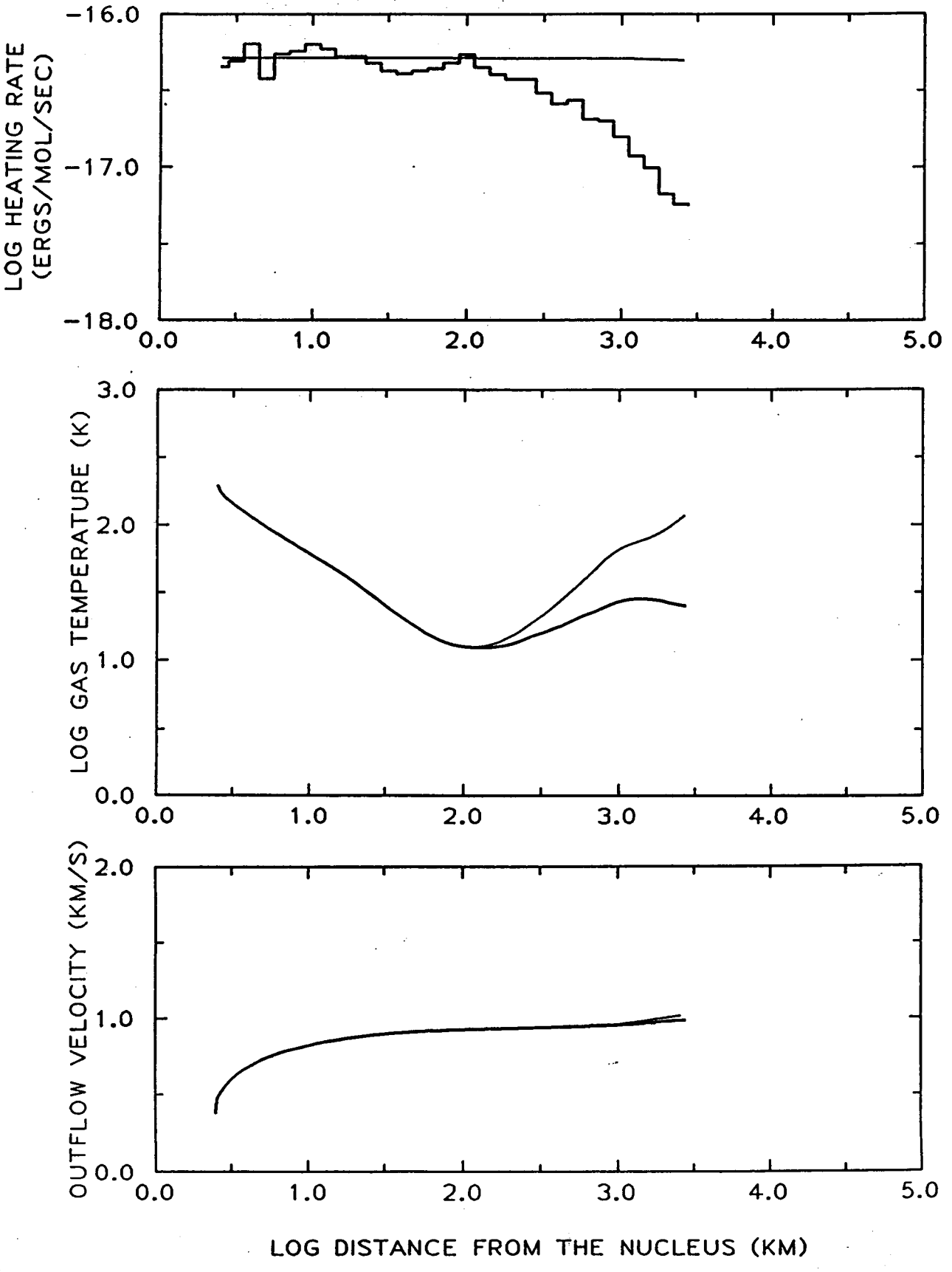
LOG HEATING RATE
(ERGS/MOL/SEC)
-16.0
-17.0
-18.0
0.0
1.0
2.0
3.0
4.0
5.0
LOG GAS TEMPERATURE (K)
3.0
2.0
1.0
0.0
OUTFLOW VELOCITY (KM/S)
2.0
1.0
0.0
LOG DISTANCE FROM THE NUCLEUS (KM)

FIGURE 5

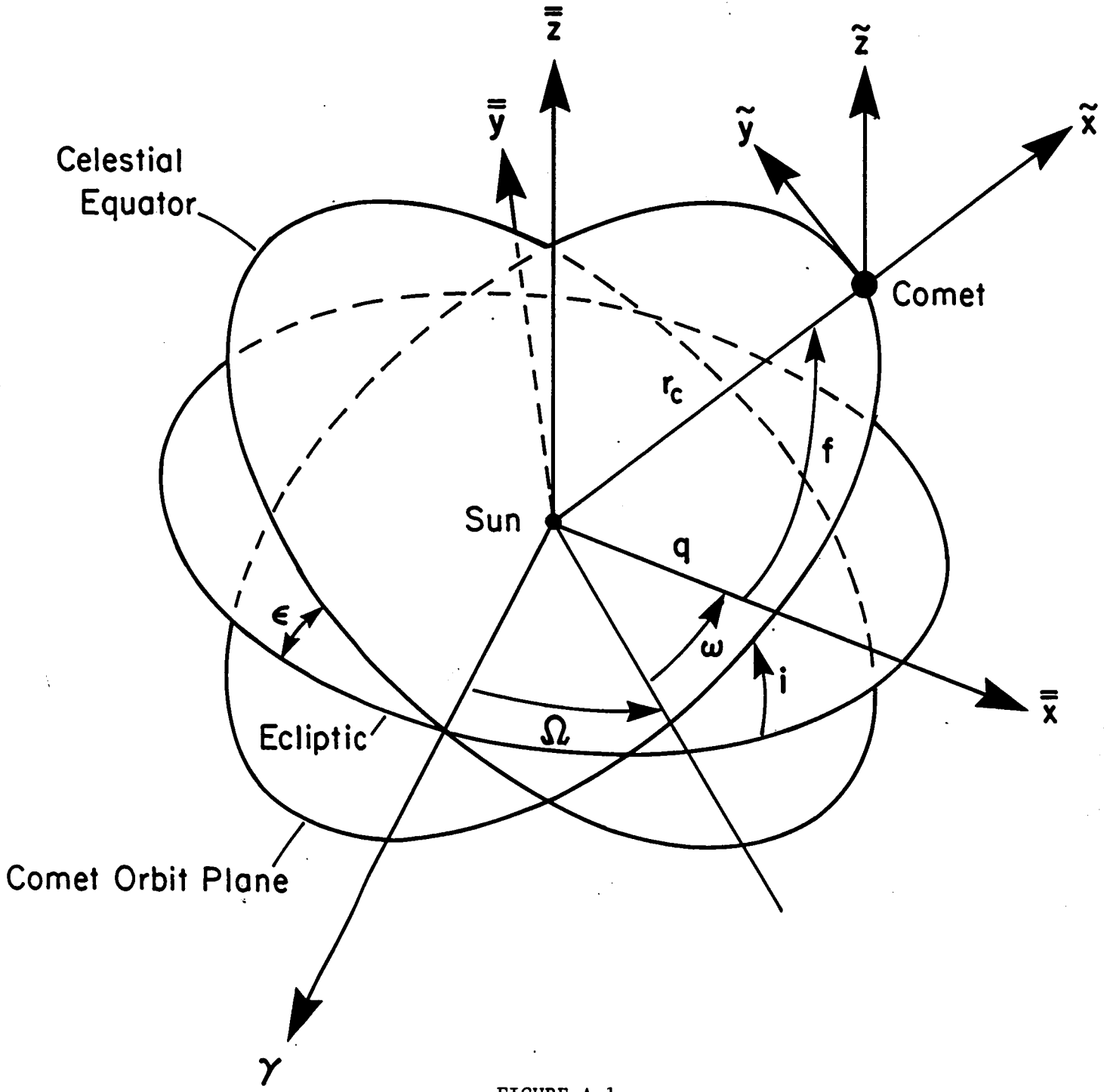
Celestial
Equator
Comet
Sun
Ecliptic
Comet Orbit Plane
$\bar{z}$
$\bar{y}$
$\bar{x}$
$\tilde{z}$
$\tilde{y}$
$\tilde{x}$
r_c
f
q
ϵ
ω
i
Ω
γ

FIGURE A.1

Monte Carlo Particle Trajectory Models for Neutral Cometary Gases

II. The Spatial Morphology of the Lyman-α Coma

by

Michael R. Combi

and

William H. Smyth

Atmospheric and Environmental Research, Inc.

840 Memorial Drive

Cambridge, MA 02139

October 1987

Abstract

The Monte Carlo particle trajectory model (MCPTM) developed in Paper 1 is applied to explain the observed morphology of the spatially extended Lyman-α comae of comets. The physical processes and assumptions used in the model as they relate to the photodissociation of H_2O and OH and the solar radiation pressure acceleration are presented herein. For this first application, the rocket and Skylab images of the Lyman-α coma of comet Kohoutek were chosen for study. The self-consistent modeling analysis of these data consisted of two parts. The first part entailed using a steady-state spherically symmetric inner coma MCPTM coupled with a simple gas-dynamic model to calculate the physical development of the coma, i.e. the dependence of coma temperature and outflow speed on radial distance to the center of the nucleus, as a function of the (time) heliocentric distance of the comet. The inner coma MCPTM was used to calculate correctly the photochemical heating of the coma due to the partial collisional thermalization of the hot hydrogen atoms produced in the photodissociation of water molecules. In the second part of the analysis the results from the first part were used in a fully time-dependent and three-dimensional extended coma MCPTM which includes the explicit calculation of partial thermalization of the H atoms by multiple collisions with coma molecules.

The same physical model yielded very good matches between the modeled Lyman-α isophotes and those observed in both of the two very different images of comet Kohoutek. The production rate was varied in time as implied by the shape of the visual light curve. All other physical parameters were varied only according to their naturally expected heliocentric distance and velocity dependencies. The complete physical description of the inner coma provided by the coupled gas-dynamic/MCPTM calculation was needed to obtain a good fit to

the data. The correct inner coma description is important since it provides not only the initial conditions for the photodissociated H atoms but also (and most importantly) the collisional targets for the H atoms produced in the innermost regions of the coma. Simplistic descriptions for the coma (single speed, and perfectly radial molecular motion) do not yield realistic isophote contours. The implications of the model results as they apply to other comets, species and a variety of conditions are also discussed.

I. Introduction

The time-dependent syndyname models developed by Keller and collaborators (Keller and Thomas 1975, Keller and Meier 1976) have been successful in being able to reproduce the shape and the radial gradient of the observed Lyman-α coma (Meier et al 1976, Meier and Keller 1980). As has been discussed in a more general context in the accompanying paper (Combi and Smyth 1987b, hereafter Paper 1), the models of Keller and collaborators consider the source of hydrogen atoms to be an isotropic point source which follows the syndyname as projected on the sky plane in order to approximate the combined effects of solar gravity and solar radiation pressure on the atom trajectories. In order to reproduce shapes of the two-dimensional sky-plane isophotes as observed in resonantly scattered solar Lyman-α emission, they required the use of the superposition of two or three Maxwell-Boltzmann distributions for the outflow speed of H atoms. Also, the H atoms must have an exponential decay lifetime of $\simeq 2 \times 10^6$ seconds at 1 AU from the sun. This value for the average lifetime can be reasonably well accounted for by the combined decay rates due to charge exchange by solar wind protons, photoionization and impact ionization by solar wind electrons (with charge exchange being the most dominant), although the actual value can vary considerably with time about the average value (Combi, Stewart and Smyth 1986). On the other hand, it is not so easy to account for the required outflow speed distribution.

It had been demonstrated that, based on circumstantial evidence, the bulk of the H atoms and OH radicals observed by their spectral emissions in cometary comae are produced by the photodissociation of water molecules (Keller and Lillie 1974) which were originally vaporized from the cometary nucleus. Furthermore, the shapes of the visual light curves of comets are consistent with vaporization which is controlled by water ice at the level generally

inferred from the H and OH abundances (Delsemme 1973). The in situ observations of comet P/Halley (Balsiger et al 1986, Krankowsky et al. 1986) have entirely confirmed this idea. The photodissociation of H_2O molecules by solar radiation has most recently been studied in detail by Festou (1981b). It is predicted that the photodissociation is highly exothermic, and that most of the excess energy is in fact imparted in the form of translational energy to the fragments. Nearly 90% of the water dissociated produces H + OH where the H atoms have a speed distribution which peaks sharply near 20 and 30 km/s. The predissociation of OH by solar photons into the v'=2 and higher vibrational levels of the $A^2\Sigma^+$ state has been studied in detail by Schleicher (1983, also see Schleicher and A'Hearn 1984) and is believed to be its main destruction mechanism. This process is also energetically exothermic and should produce H atoms with a speed distribution sharply peaked near 8 km/s. More recently, van Dishoeck and Dalgarno (1984) have presented the results of ab initio calculations which suggest that absorption of more energetic solar photons into higher lying predissociation states result in an additional rate which is somewhat smaller but comparable to the rate for the lower lying state. The higher energy dissociations are also exothermic and produce faster H atoms with speeds of 17 to 26 km/s.

The model analysis of two H Lyman-α images of comet Kohoutek taken by Meier et al. (1976) on 25 December 1973 and 8 January 1974 when the comet was 0.18 and 0.43 AU from the sun respectively, implied that the shape and the radial gradient of the brightness can be reproduced by an effective outflow speed distribution which is formed by the sum of three Maxwell-Boltzmann distributions, at 4, 8 and 20 km/s. The existence of speed components at 7 and 21 km/s had been suggested in older work by Keller and Thomas (1975) on comet Bennett (1970 II). Speeds of this order are also generally consistent

with the doppler widths of cometary hydrogen line profile data (Huppler et al. 1975, Festou et al 1979). All taken together these results were highly suggestive of a major role of H_2O and OH photodissociation in the production of observed cometary H, however many details still needed to be understood. In addition, the question of how to best model observations of hydrogen in less productive comets in general and all comets at moderate to large heliocentric distances remains in question, even if something similar to the weighted sums of Maxwell-Boltzmann distributions are reasonable for productive comets at small heliocentric distances (like Kohoutek).

Simple direct photodissociation should produce a speed distribution dominated by sharp peaks and should produce a hydrogen coma having a peculiar observable character when the atoms are subjected to solar radiation pressure (Keller and Meier 1980). Furthermore, no direct account can be made for the substantial low speed component required for the 25 December image of comet Kohoutek and the small low speed component required for the 8 January image. Meier et al. (1976) suggested that at least the existence of a low speed component could be explained by the thermalization of those H atoms produced well inside the innermost cometary coma. In fact, Kitamura et al (1985) demonstrated with a simple steady-state multiple-collision Monte Carlo model that, for a productive comet at a small heliocentric distance, a measurable thermalized component should result.

In this paper we present the results of our reanalysis of the two Lyman-α images of comet Kohoutek taken by Meier et al. (1976) with our three-dimensional time-dependent Monte Carlo particle trajectory model (MCPTM). The MCPTM includes for the first time a truly physically realisitic description of the detailed production mechanisms and trajectories of H atoms produced by the photodissociation of H_2O and OH. The MCPTM takes into account in a self-

consistent fashion the combined effects of the multiple collisions of H atoms with the outflowing coma gas and the trajectories of the atoms in the presence of solar radiation pressure and solar gravity. The results presented in this paper represent only the most recent step in an evolutionary process that we necessarily followed in order to develop a physically realistic model which could reproduce the observed 2-D isophotes of the Lyman-α coma. This process should at least be briefly described here in order to provide a clear framework for understanding the current level of complexity in our modeling efforts.

As discussed above, the past attempts to model the observed distributions of cometary hydrogen have fallen into two classes: steady-state inner coma models (e.g. Festou et al. 1979, Kitamura et al. 1985), and time-dependent and (quasi-) three-dimensional extended coma models (Keller and Meier 1976). Our broadly based goal has been to use the power and flexibility provided in the Monte Carlo method, in order to combine a physically realisitic inner coma model, generalized to include time dependence, with a true three-dimensional extended coma model in order to establish a clear physical basis for the spatial morphology of the observed Lyman-α coma.

The first step in this process was to merge the simple Monte Carlo model developed by Combi and Delsemme (1980a), which could describe the photochemical production of hydrogen from H_2O and OH with the correct isotropic ejection of daughter fragments upon dissociation, with the three-dimensional time-dependent trajectory calculation and comet-atom projection geometry, appropriate for hydrogen atoms traveling under the combined influence of solar gravity and radiation pressure. The extended coma portion of the model alone represented a technical improvement over the syndyname model of Keller and Meier (1976) in that the physical processes such as lifetimes and emission

rates did not have to be given average values for a column or at the position of the nucleus but could be included explicitly for each atom at each location in space and for the entire time history of the development of the coma.

A collision routine based on a simple single-speed perfect radial outflow for the coma gas, similar to that of Kitamura et al. (1985), was then incorporated into the inner coma portion of the model in order to account for the partial thermalization of hydrogen atoms by multiple collisions with the outflowing coma gas. The inner coma calculation of course had to be generalized to account explicitly for the time-dependent lifetimes (scale lengths) and production rate (see section II in Paper 1), as well as the Delsemme (1982) law for the heliocentric distance dependence of the parent molecule outflow speed. Once leaving the inner coma the trajectories of the H atoms in the extended coma were then calculated explicitly in three dimensions.

Although the steady-state inner coma Monte Carlo models of Kitamura et al. (1985) seemed to account roughly for the necessary fraction of low speed hydrogen atoms they made no attempt to reproduce particular observed isophote contours and only presented very crude speed distribution functions. In our first attempts to reproduce the real observations of Meier et al. (1976) we found that the simplisitic description of the coma consisting of a single-speed perfectly radial outflow for the coma molecules necessarily produced thermalized hydrogen atoms having the same perfect radial outflow speed as the coma (1-2km/s using the Delsemme velocity law). These extremely low speed H atoms produced an extremely narrow extended tail not seen in the observations. The speed distribution functions of Kitamura et al. were only computed with resolution of 5 km/s so the dominance of the extremely low speeds was not apparent. A contributing factor which had been overlooked was that even for fairly modest coma temperatures (<100 K) the thermal speed component for H

atoms is at least comparable to the radial outflow speed. For the higher temperatures expected for comet Kohoutek at 0.18 and 0.43 AU (for the two observed images) the thermal speed components should be much larger. It became apparent that some accounting for not only the outflow speed of the coma but also for the coma temperature must be included in a collisional model for the production of H atoms.

The first attempt at including a coma temperature was to assume that for each of the two images of the comet a single effective time-independent temperature could be used for the coma gas. At each collision the target coma molecule was given both its radial speed plus a randomized thermal component (randomized in both direction and across the Maxwell-Boltzmann distribution as discussed in section II of Paper 1). This simple picture was a tremendous improvement in the ability to reproduce realisitic looking isophotes for both images. It was therefore clear that the physical state of the inner coma (temperature and outflow speed) was an important shaping mechanism for the Lyman-α coma. In fact, it was apparent that for comets where collisions between H atoms and the coma are important (productive comets at small heliocentric distances) that the shape of the hydrogen coma was in fact diagnostic of conditions in the inner coma.

Ambiguities unfortunately remained since it was clear that the coma temperature varied both with time (heliocentric distance) and with distance to the nucleus and since reasonble reproduction of the observed Lyman-α isophotes could be made by a range of combinations of the outflow speed and temperature for the coma. Looking to the published results of the hydrodynamic models for the inner coma (Marconi and Mendis 1982, 1983, 1984, Huebner and Keady 1983, Ip 1983, Crovisier 1984) proved to be of little help. Only very few cases had been studied. These were usually for productive comets at 1 AU from the sun

and no systematic study of the heliocentric distance variations had been published. Furthermore, because of its collisional effect on hydrogen atoms, the region of the coma, which is of the utmost importance to characterize, is the transition region from collision-dominated flow to free collisionless flow. This is the region where the hydrodynamic models are no longer applicable.

This point had been first emphasized by Ip (1983) who pointed out that the main heating mechanism for a water dominated coma is the collisional thermalization of the hot H atoms produced in the main (90%) photodissociation branch of water. Owing to their small mass many collisions between H atoms and the heavier coma gas molecules (H_2O, CO, OH, O, etc.) are needed in order to thermalize completely. Thus the so-called photochemical heating of the coma will become inefficient even well within the traditionally defined collision region. Although Ip (1983) suggested an analytic approximation to this collisional decoupling, both Ip and later Crovisier (1984) suggested that the best way to treat this problem is with an explicit Monte Carlo collisional model. Since a collisional routine for the inner coma model had already been developed it was possible not only to calculate the effect of the collisions on the distribution of a daughter species but also to calculate explicitly the energy transfer at each collision to the coma. This energy transfer for the many collisions modeled is in fact the photochemical heating calculated at the kinetic level.

It became evident that there were important interrelations between (1) collisional thermalization and decoupling of hot H atoms (2) photochemical heating and physical development of the coma and (3) the effective (and time-dependendent) speed distribution of H atoms leaving the inner coma. An iterative scheme was therefore developed that coupled the collisional steady state inner coma MCPTM which calculated correctly the photochemical heating

efficiency to a simple gas-dynamic model which calculated the outflow speed and temperature of the coma. Preliminary model results for comet Halley using the coupled gas-dynamic/MCPTM were presented by Combi (1987), however, a more detailed description as well as a more general application is presented in section IV of Paper 1.

The results of the last iteration of the general study of the spatial morphology of the hydrogen coma, prior to the results contained in this paper, were presented in preliminary form by Combi and Smyth (1987a) as the first self-consistent calculation which included a time-dependent description of the physical state of the coma. The gas-dynamic/ MCPTM procedure was used to calculate the coma temperature and outflow speed for a number of heliocentric distances of comet Kohoutek. These results were used to infer a set of single effective coma outflow speeds and temperatures in the collision transition region where the last several collisions occur between the H atoms and the outflowing coma. The fact that the coma temperature and outflow speed depend not only on time but also on the distance to the center of the nucleus was not included. In this attempt very good reproduction for the image recorded on January 8, 1974 ($r = 0.43$ AU) was obtained, however the fit of the image of December 25, 1973 ($r = 0.18$ AU) was not quite as good.

As will be presented in section IV of this paper, the coma temperature in the region where the hydrogen atoms undergo their last few collisions, (about 10^4 km in cometocentric radius) when the comet is near perihelion, is characterized by a fairly steep drop with increasing distance. Owing to the preference for radial escape, even from fairly deep within the traditional collision zone (see Figure 3 in Paper 1), compounded by the large number of collisions required to alter the speed of the light H atoms, we found that using a single average temperature in this region does not produce the correct effective

speed distribution for the partially thermalized H atoms exiting the inner coma. Furthermore, the outflow speed of the coma, which influences the number of collisions through its effect on the gas density (through the continuity equation) and also through the dissociation scale lengths (i.e. how far out into the coma the H atoms are produced), also varies with distance from the nucleus. It became clear that a completely time-dependent description of the whole radial dependence of both the outflow speed and temperature of the coma would be required to yield a true self-consistent calculation.

The remaining sections of this paper deal with the specific application of the MCPTM tools developed in Paper 1 to the production of cometary hydrogen and to the interrelated aspects of the physics of the inner coma and the 2-D spatial morphology of the extended Lyman-α coma. Section II of this paper describes the detailed physical processes relevant to the production of cometary hydrogen as included in the MCPTM. This discussion deals with the photochemical chain for the production of cometary hydrogen atoms, the solar Lyman-α emission, collisional cross sections, and the variation of production rate with heliocentric distance. Section III describes the heliocentric distance dependent inner coma description for comet Kohoutek as modeled with the coupled gas-dynamic/MCPTM procedure discussed in Paper 1. In section IV the application of the MCPTM to the two-dimensional sky-plane images of Meier et al. (1976) are presented and are compared with the earlier modeling efforts. Also discussed in section IV are the implications of the success in modeling these data on the appropriate models to be used for analyzing data from other comets and other cometary conditions. Finally, section V presents a brief summary of results contained in this paper as well as a discussion of further improvements in and other applications of the current MCPTM to be undertaken in the future.

II. Physical Processes Included in the MCPTM

Owing to the inherent flexibilty afforded by the many-particle Monte Carlo simulation, it is possible to include explicitly the detailed space, time and velocity dependencies of the physical processes relevant to the production, kinematics and decay of hydrogen atoms in the cometary environment. Separate discussions are presented in this section of the paper regarding the photochemistry of H_2O and OH, the solar Lyman-α line profile and absolute flux, the composition and the variation of gas production rate of comet Kohoutek, the collisions between atoms and molecules, and the decay lifetime of hydrogen.

Photochemistry of H_2O and OH

The photochemistry and expected photochemical kinematics associated with the production of hydrogen in comets has been studied in detail by several other investigators. The purpose of this discussion is simply to document these details as adopted in the MCPTM analyses presented in this paper. Festou (1981b), as mentioned earlier, has studied in detail the various branches of the photodissociation of H_2O by the solar ultraviolet radiation field. In addition to assessing the rates of the various branches he has calculated the excess energy left after the exothermic photodissociation which is shared in the form of kinetic energy between the fragments. According to the results of Slanger (1982) a minor revision to the branching ratio between the OH + H and the $O(^1D)$ + H_2 for the solar Lyman-α contribution is required. Otherwise we have adopted the results of Festou (1981b) to describe both the rates as well as the speed distributions for the fragments. These results are presented in Table 1. The largest component to the direct source

of H atoms at 20 km/s is actually the narrow Gaussian distribution at 19.6 km/s as determined by Festou, and is included as such in the model.

The main photodecay process for OH radicals is actually a predissociation from the ground state to the v'=2 and higher vibrational levels of the $A^2\Sigma^+$ state. The transition to the v'=1 vibrational level results in the familiar observed fluorescent transition at 3090 Å. The predissociation process was examined in great detail by Schleicher (1983, also Schleicher and A'Hearn 1984), who calculated not only the dissociation rate but also the heliocentric velocity dependence of the rate. This velocity dependence results from the Swings effect, since the solar spectrum is dominated by many absorption lines (most due to solar OH) whose positions vary relative to the cometary OH rotational lines with different doppler shifts. An additional predissociation process has been suggested in the results of van Dishoeck and Dalgarno (1984) whose ab initio quantum mechanical calculations have identified the existence of higher lying states which can be populated by the absorption of solar Lyman-α. They have combined their results for these newly identified transitions with the earlier work of Schleicher to present a complete picture of the photodissociation rate of cometary OH as well as the energetics of the H and O atoms produced.

The absorption of the long wavelength solar UV photons into the $A^2\Sigma^+$ state should produce H atoms having excess speeds primarily of 8 and 11 km/s, however the higher lying states should produce much faster H atoms with speeds of 17-26 km/s. In addition, the results of van Dishoeck and Dalgarno (1984) also predict the production of a large number of O atoms in the ^1D state which should produce a much larger spatially extended (although faint) emission of the familiar 6300 Å forbidden line that has typically been observed as concentrated in the inner coma and attributed to one of the primary

photodissociation branches of H_2O (see Table 1). In recent work by Roesler et al. (1987), the emission of the 6300 Å line at nearly 10^6 km from the nucleus of comet P/Halley at a level consistent with all of the projected branching ratios may be a confirmation of the ab intio calculations of van Dishoeck and Dalgarno. Table 2 shows the photodissociation rates and excess speed distributions adopted in the MCPTM for the OH photodissociation. The expected heliocentric velocity dependence of Schleicher (1983) for the $A^2\Sigma^+$ absorption has been explicitly included.

The speed distributions for the H atoms and OH radicals from all photodissociation branches in Tables 1 and 2 are spanned in the MCPTM as discussed in section II of Paper 1. The probability distribution function of the excess speed was constructed for each photodissociation process, so that given a random number on the interval from 0 to 1 a proper speed for an OH radical or an H atoms is chosen according to Eq. 17 in Paper 1. The photodissociation rates contribute to the decay lifetimes for H_2O and OH and are included in the model with their full time (heliocentric distance) dependences according to the procedure given by Eq. 5-12 in Paper 1. The heliocentric velocity dependence for the OH lifetime is evaluated according to the time dependence of the heliocentric velocity of the nucleus, since the changes in the lifetime are small compared with the dispersion of the speeds of the OH radicals in the nucleus (1-2 km/s). This effect could be treated with the MCPTM, but is a needless complication at this point.

The Solar Lyman-α Flux and Line Profile

The solar Lyman-α radiative flux serves both as the primary source of the radiation observed from the hydrogen coma as it is resonantly scattered from the atoms, and (through this scattering) as the source of the radiation

pressure acceleration felt by the H atoms as they move in their orbits away from the comet around the sun. In fact, depending on the level of the variable solar flux and on the doppler shift of a cometary H atom relative to the solar line profile, the radiation pressure acceleration on H atoms ranges from somewhat below to somewhat above the solar gravity acceleration. The proper estimation of both the solar Lyman-α line profile shape and also the total integrated line flux is of the utmost importance in modeling both the production rate of hydrogen (through the photon emission rate or g-factor) as well as the speed distribution of atoms exiting the inner coma (through radiation pressure acceleration which causes the observed spatial distortion in the shape of the isophote contours).

The estimate of the Lyman-α flux at line center adopted in the early cometary hydrogen work (Keller and Thomas 1975, Meier et al. 1976) of 3.7×10^{11} photons cm^{-2} s^{-1} $Å^{-1}$ for the solar minimum conditions appropriate in the period of 1973-1974 is about 40% higher than current estimates of the appropriate value (Lean and Skumanich 1983). There has been some controversy over the absolute calibration of different instruments during the last ten years although the lower values seem more reasonable. We also now know that the actual solar flux in Lyman-α can vary by $\pm$10% over a single 27-day solar rotation period. Although it is now possible to assess the day-to-day changes in the value by appropriate time shifts (solar rotations) of Solar Mesospheric Explorer measurements there are no such data available for the period covered in the Kohoutek observations. Therefore, we are required to adopt the new average estimated value (2.75×10^{11} photon cm^{-2} s^{-1} $Å^{-1}$ for the line center flux and 2.5×10^{11} photons cm^{-2} s^{-1} for the integrated flux) and to keep in mind that variations of the order of 10% may effect the overall production rate as well as the radiation pressure acceleration.

The solar Lyman-α emission is concentrated in a line whose FWHM is of order 1 Å and whose line center is self-reversed by about 35% from the maximum flux. A full solar disc Lyman-α profile was constructed by Lemaire et al. (1978) from an observed high resolution disc-centered and limb spectra. This spectrum is reproduced in Figure 1 with the original geocoronal absorption line filled-in to approximate the line as seen by a hydrogen atom in a cometary coma. In the MCPTM the resonance scattering rate for a hydrogen atom is calculated given the doppler shift for the appropriate heliocentric velocity and where the integrated line flux, as shown in Figure 1 is scaled to the desired value. For example, in the model results published for comet P/Giacobini-Zinner (Combi, Stewart and Smyth 1986) the integrated solar line flux determined from the measured SME data was used to scale the entire line profile. For the results presented in this paper the integrated flux of the Lyman-α line constructed by Lemaire et al. (1978) from observation has been scaled down linearly to the adopted value. Here too there has been some disagreement in the literature as to whether the integrated flux scales linearly with the flux at line center or with some power (Vidal-Madjar 1977). However, long term observations of interplanetary hydrogen do support the linear scaling (Shemansky 1986). The actual calculation of the photon emission rate and radiation pressure acceleration from a given solar flux is a well-known relation (see e.g. Keller and Meier 1976) and will not be discussed here.

The Gas Production Rate Variation and Composition of Comet Kohoutek

For the purposes of the modeling analysis presented in this paper the adoption of both the variation in time of the water production rate as well as a crude estimate of the basic gas composition is necessary. As has been

discussed in the past by many investigators, time dependences in the production rate, decay lifetimes and the solar Lyman-α flux likely effect the observed morphology of the hydrogen coma in a convolved manner. Without independent measures of the day-to-day variations in the solar UV flux, and the solar wind flux it is not theoretically possible in a modeling context to separate the intertwined effects of variable lifetime and variable production rate, although estimates of the longer term averages of these variables can certainly be obtained. The composition is important for the coupled gas-dynamic/MCPTM calculation of the coma dynamics since the mean molecular mass of the coma gas must be estimated not only for the H_2O which eventually produces the H coma but also for the likely presence of CO and CO_2 in non-negligible amounts. The contribution to the total density is also needed for the collision calculation for the H atoms in the extended coma MCPTM, since the addition of 20% of species other than water will decrease all collision paths by about 20%, increasing the heating efficiency over a pure water coma.

In the hydrogen models of Keller and Meier (1976), one of the adjustable parameters in the data fitting procedure is the form of the gas production rate time variation law. Meier et al. (1976) assumed that the gas production rate, Q, varied in time with the heliocentric distance, r, according to the commonly assumed power law, $Q=Q_0 r^n$, where Q_0 is the production rate at 1 AU and n is an adjustable parameter. For each observation (which included the two full images we address here, in addition to a set of poor quality images that were reduced to upsun and downsun radial profiles) they computed a value for Q and n. The upsun and downsun radial profiles are not good indicators of the correct outflow speed distribution in the model of Keller and Meier. As a result they published a set of H production rates which provided, in effect, the heliocentric distance dependence of the production rate. However, owing

to large calibration uncertainties in the larger set of poor quality images, as well as some of the parameter ambiguities, it would be difficult to draw firm quantitative conclusions regarding the variation of the gas production rate. Furthermore, apparent variations in the H production rate could have been due rather to real day-to-day variations in the solar Lyman-α flux.

Another approach, which we have adopted here, is to examine the variation in gas production rate as inferred from the visual light curve of comet Kohoutek. Delsemme (1976) published an analysis, in which he fitted a theoretical vaporization curve to a compilation of many visual magnitude estimates. For the purpose of this study, the reduced magnitudes of Delsemme's compiled pre- and post- perihelion light curves have been converted to the relative time variation of the gas production rate. Figure 2 shows the smoothed results of our adopted production rate variation normalized to the production rate at 1 AU pre-perihelion, Q_0. During the build-up time for the hydrogen coma observed in the two Lyman-α images (.43 AU pre-perihelion to .43 AU post-perihelion), the variation in production rate has a power law slope in the range of 2 to 3 with a noticeable post-perihelion dimming. The broad general trend is at least somewhat similar to the variation inferred by Meier et al. (1976) from bulk of the poorer quality upsun and downsun Lyman-α profiles.

This assumed gas production rate variation had been reasonably well reproduced by Delsemme's (1976) vaporization theory which assumed a volatile composition of 85% water and 15% of a more volatile substance. This is not unlike the composition which can be inferred for the in situ and remote observations of comet P/Halley (Krankowsky et al 1986, Balsiger et al. 1986, Stewart 1986, Feldman et al. 1986). With all of this in mind we have adopted a gas composition for comet Kohoutek which is 80% H_2O, 16.5% CO and 3.5% CO_2.

The main effects of the assumed composition are in the mean molecular mass for the coupled gas-dynamic/MCPTM and in the coma gas collision cross section in both the former and the extended coma MCPTM.

Hydrogen Lifetimes and Collisions

The last two physical processes of importance in shaping the distribution of hydrogen in the extended coma are the decay lifetime of hydrogen atoms in the coma and the mechanical description of collisions between atoms and molecules. As discussed in section I of this paper hydrogen atoms in the interplanetary space around the cometary nucleus may be effectively removed from the coma by three main processes: 80% by charge exchange by solar wind protons, 15% by photoionization by solar UV photons, and 5% by electron impact ionization by solar wind electrons. Although the canonical value of 2×10^6 seconds for the total lifetime of hydrogen can be derived from mean solar extreme UV fluxes, and solar wind density and bulk flow velocity, these conditions are known to vary widely on time scales short comparable to the lifetime itself. The lifetime of hydrogen atoms has been calculated, using data recorded by the ICE satellite during the 42-day period prior to its encounter with the tail of comet P/Giacobini-Zinner, by Combi, Stewart and Smyth (1986) for the purpose of the MCPTM analysis of Pioneer Venus observations of the Lyman-α coma. It was found that although the 42-day average was nearly identically equal to the canonical value, the running 12-hour averages of the lifetime varied over a range from as small as 2×10^5 up to 3.5×10^6 seconds.

For the purpose of analyzing the comet Kohoutek data (or that of most other comets for that fact), it is impossible to reconstruct such a detailed picture of solar wind conditions needed to calculate the hydrogen atom

lifetime. Therefore as in the earlier studies we are forced to adopt the constant average value. What is important to note however is that, when assuming a single constant value for the lifetime in a model (scaled appropriately with heliocentric distance), real variations in lifetime are not easily distinguished from variations in production rate. The real lifetime variations can be large, and the departures from the average last long enough to cause easily detectable effects on the observed abundance and distribution of hydrogen atoms.

As discussed in section II of Paper 1, both the inner coma and extended coma MCPTM explicitly calculate the effects of many collisions for the daughter H atoms and also OH radicals with the background outflowing coma gas. Each collision has been assumed to be a hard-sphere elastic collision. Although this is a fairly simplistic description, it is reasonably appropriate for these low to moderate energy collisions between atoms and molecules (Johnson 1982). The collision cross sections between atoms or molecules may be well approximated by the sums of the individual atom cross sections as determined from the individual atomic radii, which are 0.6 Å for O atoms and 0.7 Å for H atoms (Allen 1973). These estimates yield total collision cross section of 1.89×10^{-15} cm^{-2} for H onto H_2O, and 3.24×10^{-15} cm^{-2} for OH onto H_2O. These are comparable to the typical values quoted in the literature in discussions of cometary collision zones (Festou 1981a, Ip 1983, Crovisier 1984).

For these first results presented in this paper and Paper 1, we have assumed all collisions occur between the modeled daughter species (H for example) and a molecule having the mean molecular mass resulting from the assumed chemical composition. This is a very good approximation if in the region where many collisions occur most of the parent molecules have not yet

dissociated, which is in fact true except in extreme cases of large gas production rate and small heliocentric, as was illustrated in Figure 1 of Paper 1. It is only when comet Kohoutek was near perihelion that we approach such a limit. However, as the results in the next section of the paper show, since collisions were dominant out to large distances from the nucleus the pure gas-dynamic description is applicable for Kohoutek near perihelion and all species are collisionally coupled to one another anyway. Therefore, our description of the outflow speed and gas temperature remains valid, and since the collision cross sections are calculated as the sums of the individual atomic cross sections the collision path lengths are calculated correctly in the MCPTM.

The only uncertainty which remains then is that for the time near perihelion the H atoms may have been thermalized a bit too rapidly by not accounting for collisions between an appropriately partitioned set of species. The inclusion of this effect would necessitate the modeling of the detailed kinetic theory for individual species (H_2O, OH, H, O etc.) and would entail a tremendous complication of the model far beyond the scope of these papers. On the other hand, the general question of the collisional decoupling of individual species from each other and of particles in one species from themselves represents a fundamentally important problem which the general MCPTM method as derived in Paper 1 can ideally address at the kinetic theory level. This question will be left for future work.

III. The Inner Coma of Comet Kohoutek

Using the iterative approach developed and discussed in section IV of Paper 1, the coupled gas-dynamic/MCPTM was used to calculate the physical development (outflow speed and gas temperature) of comet Kohoutek at various times previous to the two Lyman-α observations which was the goal of the modeling analysis. This type of analysis would provide the necessary time history important for calculating the correct trajectories for H atoms in the coma of the comet. The gas-dynamic/MCPTM uses the steady-state inner-coma MCPTM (see section IV of Paper 1) to calculate explicitly the photochemical heating rate of the coma by the most dominant process (by far) which is the collisional thermalization of hot H atoms produced by the primary photo-dissociation branch of water. A steady-state model for the inner coma can be used since the dynamical time scale important for building up the collision and transition zone region of the coma (about 10^5 seconds) is small as compared with the time scale involved in changes in cometary conditions due to changes in heliocentric distance. These heating rates are then used in a single-fluid multi-species gas-dynamic model which calculates the outflow speed and temperature of the coma. The new outflow speed and temperature profiles are then used in the MCPTM to calculate new heating rates, and the procedure is iterated until a convergent solution is reached. Since the collisional inner coma MCPTM is the more computationally intensive of the two procedures, the first iterations are made with a low statistics MCPTM (fewer total particles). As the iteration proceeds the number of molecules is increased.

As discussed in section I of this paper the final versions of the Lyman-α images as modeled here are the result of an evolutionary process which involved less complicated (and less self-consistent) modeling attempts.

The gas production rate variation was adopted from the visual light curve of comet Kohoutek (see previous section and Delsemme 1976). Both the details of the collisional thermalization efficiency in the coupled gas-dynamic/MCPTM and the final outflow speed distribution of H atoms exiting the inner coma in the extended coma MCPTM obviously depend on the total gas production rate. The larger the total gas production rate is, the more efficient the collisional thermalization will be and the more H atoms will be partially thermalized and slowed from their initial photodissociation speeds. However, from previous reasonably successful reproductions of the 2-D isophote shapes of the January 8, 1973 image of the comet (r = 0.43 AU), the appropriate value of the normalization factor for the time dependence of the production rate, Q_0, in Figure 2 was fairly well specified.

Therefore, for the results presented here the appropriate time dependence of the gas production rate could be adopted from this value. Table 3 shows the adopted parameters for five gas-dynamic/MCPTM analyses of the physical development of the inner coma of comet Kohoutek which span a 16 day period prior to the image recorded on January 8, 1974, and cover the required backup time to generate the whole Lyman-α coma for both observations. We chose the perihelion time for one of the times as well as two pairs of heliocentric distances on either side of perihelion, one set by the heliocentric distance at the later of the two images (0.43 AU) and one intermediate (0.25 AU). It is not possible to use redundant results for the same heliocentric distances on either side of perihelion because the production rate curve is higher before perihelion than after and the photochemical heating efficiency depends upon the absolute production rate. Furthermore, having results for the same heliocentric distance but different production rates provides an interesting comparison of the theoretical results themselves.

The total gas production rate was set for a self-consistent production of the observed Lyman-α emission according to the chemical composition adopted for comet Kohoutek and the branching ratios of the hydrogen atoms produced in the photodissociation of H_2O and OH. The total gas production rate is then about 36% larger than the value usually taken to be one half of the hydrogen atom production rate, which implicitly assumes a 100% water composition and 100% of the water produces H + OH. Owing to their long photodissociation times, CO and CO_2 cannot contribute substantially to the heating rate within the collision zone (Ip 1983). The details regarding the functional form of the parameters (the IR cooling rates, the radiation trapping) used in the gas-dynamic portion of the calculation have been discussed elsewhere (Combi 1987, and Paper 1) and will not be reproduced here. A discussion of the limitations and possible improvements in the assumptions and the whole approach will be presented later.

Figures 3a, b, and c show the resulting dependence on the radial distance to the center of the nucleus of the coma gas temperature, velocity, and Mach number, respectively, for the five coupled gas-dynamic/MCPTM calculations. The results have been terminated at the traditional collision zone radius, that radial distance to the center of the nucleus which is equal to the local mean free path for one collision. Outside this distance, collisions between all atoms and molecules are too infrequent to drive the typical adiabatic expansion/cooling predicted by pure gas-dynamic models which gradually turns internal random kinetic energy (temperature) into larger bulk outflow speeds. As discussed in Paper 1, there is a large and gradual transition zone from collision-dominated to collisionless molecular flow extending from somewhat inside to somewhat outside the traditional collision zone radius.

The curves presented in Figure 3 contain some significant results in terms of both the production of the spatial morphology of the Lyman-α coma and also some general properties of cometary comae. In the fairly mild case of a comet with a production rate of 10^{29} s^{-1} at 1 AU from the sun, the gas temperature (after initial cooling) never reaches values greater than about 30K (Paper 1). On the other hand, when the heliocentric distance is less than 0.5 AU, the gas temperatures at some locations within the inner coma can reach values ranging from 300 K at 3000km from the nucleus at 0.43 AU to as large as 900 K at 1000 km from the nucleus at 0.14 AU. Owing to a combination of the adiabatic expansion/cooling and the collisional decoupling of the hot H atoms, however, the temperatures at the edge of the collision zone radius are always smaller than 100 K.

A heating rate efficiency may be defined as the true local heating rate (due to the increasingly insufficient number of collisions by the hot H atoms) divided by the rate assuming 100% local thermalization. Figure 5 in Paper 1 shows that the heating rate efficiency begins to fall from unity at distances of about 1/10 of the collision zone radius. Therefore, before the bulk of the heavier coma gas can become collisionally decoupled from itself (at the collision zone radius), the photochemical heating rate from the light hot H atoms falls and the adiabatic expansion and cooling dominates the flow. So, the temperatures at the collision zone radius will generally always be small. In terms of their contribution to the velocity distributions of H atoms leaving the inner coma, however, the higher temperatures inside the traditional collision zone radius are important when considering the large number of collisions required to thermalize the atoms compounded by the true directional dependence of the collisional mean free path which highly favors radial escape (see for example Figure 3 in Paper 1).

The adopted production rate variation which is asymmetric for equal heliocentric distances from pre- to post- perihelion times does have some effect of the flow dynamics, although it is only really noticeable for the pair of model results for r = 0.43 AU where the pre-to-post production rate ratio is 1.6. At 0.25 AU the ratio is only 1.1 and little difference is seen. During the preperihelion times the gas production rate is higher, the collision zone radius is larger and the resulting heating rate efficiency remains higher for somewhat larger distances from the nucleus. Interestingly the same combination discussed above of falling heating efficiency and adiabatic expansion and cooling yields a gas temperature that is the same both before and after perihelion at the collsion zone radius (which is larger before perihelion). What changes is the bulk outflow speed at the collision zone radius which is 1.70 km/s before perihelion and 1.55 km/s afterwards. This same process may be at least partially responsible for the different outflow speeds inferred from the infrared observations of H_2O in comet P/Halley at comparable heliocentric distances before and after perihelion (Larson et al. 1986).

A more general result present in these model curves is the heliocentric distance dependence of the outflow speed of the parent gas molecules. Because of the self-decoupling of the coma molecules from themselves near the collision zone radius, as discussed above, the velocity distribution of molecules outside this radius can be approximately described as the vector sum of the bulk radial speed at that radius with a small (<0.3 km/s) initially isotropic thermal component. This isotropic component will become less isotropic and eventually just a small radial distribution at distances much larger than the collision zone radius due to simple geometry. Comparing the asymptotic values of the outflow speed at different heliocentric distances we

find that they do vary approximately as the inverse square root of the heliocentric distance as in the Delsemme (1982) law. However, the value at 1 AU is not 0.58 km/s but more like 1 to 1.1 km/s. The example gas-dynamic/ MCPTM results in Paper 1 at 1 AU are consistent with this value. Recent estimates of cometary outflow speeds from various measurements of comet P/Halley are also consistent with these larger levels (Larson et al 1986, Balsiger et al. 1986).

IV. The Spatial Morphology of the Lyman-α Coma

The steady-state inner coma model results, as described in the previous section of the paper, give the dependence of the outflow speed and temperature of the principal coma gases on the cometocentric distance for five different times (or locations) of comet Kohoutek. These five snapshots were used as input conditions to characterize the time development of the coma dynamics which effects both the source kinematics and the collisional targets at a kinetic level, in the full three-dimensional time-dependent MCPTM description of the spatial morphology of the hydrogen coma. Time-dependent temperatures and outflow speeds at all locations within the coma were generated by interpolating between the five steady-state inner coma MCPTM results. Although the mathematical description of the model is given in the accompanying Paper 1 a brief qualitative summary of the extended coma MCPTM is given below.

The full hydrogen coma MCPTM actually contains two major parts. One treats the fully time-dependent inner coma in a nucleus-centered coordinate system in which displacements from the nucleus are small ($< 10^6$ km) as compared with typical heliocentric distances (10^8 km). This part contains most of the complicated physical processes, such as the collisions, dissociation times, and excess photodissociation energy, as well as the weighting scheme employed in the Monte Carlo simulation. This inner coma portion of the full hydrogen coma model is <u>completely separate</u> from the steady-state inner coma model discussed in the previous section, although many of the procedures employed in the two are similar. The second part explicitly calculates the heliocentric trajectories of the H atoms in three dimensions given their initial conditions as determined from the inner coma part, and performs the sky-plane projection of the atom taking into account the relative geometry of the earth, sun and comet at the time of the observation.

Although this full version of the MCPTM is needed to describe the time dependence and three-dimensional trajectories required to explain the morphology of the spatially extended hydrogen coma, it should be noted that the model actually provides a correct and complete description of the coma even for the smaller spatially confined inner regions of the coma. This is an important aspect which distinguishes this treatment from other models which can only be relevant to either the inner or the extended regions but not both. The reason for including this generality is that the inner coma conditions are in fact critically important in shaping the spatially extended coma. Therefore, it is useful at this point to qualitatively go through a step-by-step description of a single pair of hydrogen atom trajectories as treated in the full model.

Many primary parent water molecules are considered to be vaporized from the nucleus over a long backup time interval prior to the observation time snapshot. The emission time distribution is not skewed; the emission times for individual molecules are picked randomly on the backup time interval (Combi and Delsemme 1980a). The variable production rate is included as a multiplicative weighting factor for the contribution of both daughter H atoms. A forced dissociation time for the H_2O molecule is calculated according to the general time-dependent description for the lifetime, and the molecule is displaced from the surface of the nucleus by the appropriate distance according to time-dependent coma dynamics.

At this point the H_2O molecule is dissociated. Separate trajectories are followed for the OH radical and the primary H atom, as they are ejected from the moving center-of-mass of the H_2O molecule, which is given its appropriate local bulk radial speed and a randomized isotropic thermal component from the local gas temperature. The ejection speeds of the fragments (H and OH) are

picked according to the excess energy speed distribution of the photodissociation (Table 1). For the OH radical a forced dissociation time is also calculated using the same method as for the parent H_2O, except that the explicit heliocentric velocity dependence of the OH lifetime (Schleicher 1983, van Dishoeck and Dalgarno 1984) is also included. The OH trajectory is then calculated, collisions with the outflowing coma gas molecules are allowed to occur, and then finally the radical is dissociated at the appropriate time. Another H atom is then emitted from the moving center-of-mass of the OH according to the excess energy distribution for that dissociation (Table 2).

The trajectories of each of the H atoms (the primary from the H_2O dissociation and the secondary from the OH dissociation) are followed in a similar manner to the OH radical within the region where collisions occur. A distance of 10^6 km was adopted as an upper bound distance to separate the inner and extended coma portions of the MCPTM. Nearly all of the collisions occur at much smaller distances. The H atoms are followed in the model initially in the inner coma portion of the model to calculate the multiple collisions which occur. The typical scenario is that at some distance from the nucleus which is much smaller than 10^6 km the collision path (Eq. 32 in Paper 1) becomes infinite; at this point the initial conditions of the atom (location, speed and time) are set for the extended coma trajectory calculation. This is done by applying a fourth-order Runge-Kutta method to the modified classical two-body problem (Eqs. 34-36 in Paper 1).

For each time step (either an inter-collision time interval or a time step in the Runge-Kutta solution of the extended trajectory) the time-dependent decay weights for the H atoms are calculated according to Eq. 12 in Paper 1. At the observation time the relative projection geometry of the earth, sun, comet and atom is calculated and a sky-plane location for the atom

relative to the comet nucleus is found. For a remote observation, for example from Pioneer Venus (Combi, Stewart and Smyth 1986), the location of the earth would of course be replaced with the location of Venus. The Lyman-α emission rate is calculated for the actual heliocentric velocity and distance of the atom according to the adopted solar Lyman-α profile and integrated flux. The contribution of the atom is then added to sky-plane grids for density and Lyman-α emission having already been defined. Since the trajectories and all of the physical processes, at least for the results presented here, are symmetric above and below the comet orbit plane each atom is also reflected through this plane ($z \rightarrow -z$) and an identical contribution is added at that location. Given an arbitrary observational geometry, as is generally the case, this provides a direct gain in efficiency of a factor of two. An above the orbit plane view of the coma for a fictitous observer located at a large distance above and normal to the plane of the comet's orbit, is also saved in the model. This serves as an interesting reference point usually showing the most elongated tail.

The full hydrogen coma MCPTM, as described qualitatively above, and in detail in the previous two sections of this paper and in Paper 1, has been applied to analyze the two Lyman-α coma images of comet Kohoutek published in a paper by Meier et al. (1976). The first of the images was recorded by an electrographic camera on board Skylab on December 25, 1973 when the comet was 0.18 AU from the sun. The second image was recorded by a rocket-borne electrographic camera on January 8, 1974 when the comet was 0.43 AU from the sun. As discussed in section I, other images recorded from Skylab did not produce high quality two-dimensional images and only the upsun and downsun profiles were analyzed by Meier et al. with the model of Keller and Meier (1976).

The full isophote contour shapes and their brightness gradients for both images were successfully reproduced with the same self-consistent model based on a production rate variation determined from the visual light curve (which has been reproduced by Delsemme's (1976) standard vaporization model). All other physical processes were modeled according to their naturally expected heliocentric distance and velocity dependences. Figure 4 shows the comparison of the modeled and observed isophote contours for comet Kohoutek on January 8, 1974. The total hydrogen column densities are small enough (at least up to the 50 kR level) so that the coma is clearly optically thin. The small scale irregularies in the model contours are generally representative of the statistical uncertainties which are unavoidable in this type of analysis. However, this poses no problem here since they are much smaller in scale than the observed irregularities.

Figures 5a and b show two versions of the comparison of the modeled isophote contours for the observation of December 25. Since the column density of hydrogen is large, owing to the large production rate, it is likely that the central portion of the coma is somewhat optically thick. It is clear from the physical processes occuring in the inner coma and treated by our model, that neither a simple spherical radial outflow nor a thermally isotropic description (as are typically assumed) will provide the correct H-atom velocity distribution which is needed to calculate properly the radiative transfer of the Lyman-α photons in the inner coma. The calculation of the spherical radiative transfer problem using a realisitic phase space (space density and velocity) distribution for H atoms in the coma (as is included in our model) would be an important but difficult problem.

In order to attempt a first order estimate of the effect of radiative transfer on the Lyman-α coma, we have compared in Figure 5 the observations

both with the optically thin results and with a plane parallel correction to the radiative transfer problem (McElroy and Yung, 1975). The optically thin result should overestimate the brightness in the inner optically thick region, whereas the plane parallel correction should underestimate the brightness. This particular radiative transfer correction is for a plane parallel slab of hydrogen at a temperature of 5000 K, which corresponds to a most probable Maxwell-Boltzmann speed of 9.2 km/s which is actually quite representative of the mean speeds in the inner coma. A true spherical radiative transfer calculation should fall somewhere intermediate between the plane-parallel and the optically thin result. The comparison of the observed image with the two modeled images in fact shows that a correction generally intermediate between these two extremes would work reasonably well. A realistic radiative transfer calculation should account for the true phase space distribution which is neither thermally isotropic (like the plane parallel case) nor perfectly radial.

Another complication included in our model results for the December 25, 1973 image is that for absorption of the cometary Lyman-α emission by the hydrogen atoms in the earth's geocorona. On December 25, 1973 the comet's geocentric velocity was only 2.29 km/s. We have assumed the same transmission characteristics as a function of wavelength as used by Meier et al. (1976) in their model result for the same image. One improvement enabled by the use of the MCPTM method, which provides the actual three-vector velocity of each atom trajectory, is that the explicit transmission function was used to attenuate the emission contribution for each atom. Meier et al. used an approximate form for the assumed width of the velocity distribution of cometary H atoms along each column line of sight, given the average doppler shift of the whole

column from the syndyname model, and then integrated the transmission curve convolved with the approximate cometary emission line profile.

As has already been mentioned the same normalization factor (Q_0 in Figure 2), was used in scaling the variation of the gas production rate to its actual time-dependent variation for both image. This normalization factor sets the value of the hydrogen atom production rate at 1 AU preperihelion to be 2.7 x 10^{29} per second. This implies a water production rate of 1.47 x 10^{29} per second at 1 AU pre-perihelion, given the adopted water photodissociation branching ratios. This yields hydrogen production rates at the two observation times of 9.6 x 10^{29} at 0.43 AU and 8.4 x 10^{30} per second at 0.18 AU, as compared with 6.2 x 10^{29} and 5.5 x 10^{30}, respectively, found by Meier et al. (1976) using the syndyname model. There is really not much significance in the difference in production rate, since most of the difference is due to the fact that we adopted a smaller value for the solar Lyman-α flux based on more recent solar data. There are, however, a number of significant implications which may be drawn by the comparision of the two very different modeling analyses (presented here and by Meier et al.) both of which reproduce the shapes of the isophote contours reasonably well.

First the fundamental differences between the two models should again be stated. The syndyname models used by Meier et al. consider the source of hydrogen to be a point centered on the nucleus. For the purpose of analyzing these wide field images, this in itself is a reasonable simplification since the scale lengths for the source dissociations of H_2O and OH are not resolvable on the scale of the data. Their outflow speed distribution on the other hand is parameterized and constructed by the weighted sum of three Maxwell-Boltzmann distributions which are, for a single image, assumed to be constant in time. For the MCPTM results presented here the effective outflow

speed distribution for H atoms leaving the inner coma is not a fitting parameter but represents the natural self-consistent outcome of photodissociations and multiple collisions with a water dominated coma. Furthermore, this effective speed distribution in the MCPTM is inherently a time dependent quantity (unlike the syndyname model) since the collision rates depend in a complex way on the production rate, the photochemical lifetimes and the coma temperatures, all of which are explicitly time dependent.

A rough quantitative comparison can be made for the speed distribution functions of hydrogen atoms leaving the inner coma of the comet. It is, after all, this speed distribution, which when interacting with the relative forces of solar gravity and radiation pressure between different atoms, that creates the observed shapes of the isophote contours. Figure 6 compares the sums of the three Maxwell-Boltzmann distributions as determined by the fitting of the syndyname models by Meier et al. to the observed images, with the effective time-averaged outflow speed distribution function as calculated in the extended coma MCPTM results. This distribution was calculated in the MCPTM by determining the outflow speed of each hydrogen atom at the time the atom left the inner coma portion of the model (always $< 10^6$ km). The outflow speed distribution was binned in 1 km/s intervals and each atom's density contribution to the coma as a whole was also accumulated in the correct velocity bin. This was found to be the most directly comparable quantity to compare the MCPTM results with the parameterized distributions of Meier et al.

When comparing the syndyname results for the two different images, Meier et al. noted that a signficant population of low speed (4 km/s component) H atoms were needed in order to fit the image at 0.18 AU, but that only a small (and possibly negligible) amount was needed in order to explain the image at 0.43 AU. As the MCPTM results demonstrated, they correctly assessed the fact

that more H atoms are produced deep in the dense part of the coma where they would be thermalized. High speed components (> 20 km/s) are also evident in both sets of modeled distributions, although since we have adopted a smaller solar Lyman-α flux we have obtained a reasonable fit with essentially no atoms above 32 km/s. Both sets of model results also peak at around 8 km/s. The MCPTM distributions are however far more irregular than the smooth Mawxell-Boltzmann distributions. Although, it should be noted that Meier et al. explicitly mentioned there was no implication of a unique fit for their modeled distributions to the image data.

As discussed in section II and Paper 1, the assumption of elastic hard-sphere collisions between atoms and molecules with cross sectional diameters of order of a few Angtrom units is rather simplistic. Actual interactions are rather complex, having long range but weak attractive forces and short range repulsive forces (Johnson, 1982). In addition, the collision between an atom and a molecule is likely to be somewhat inelastic (at least in the general case) owing to the possibility of exciting internal rotational and/or vibrational states of the molecule. In the absence of measured scattering cross sections between H atoms and H_2O molecules in the appropriate energy range (0.1 to 2 eV), some general statements can be made regarding the assumption of elastic hard-sphere collisions and its effect on our model.

For the purposes of our calculation, if inelastic processes were very important then more energy could be transfered per collision. Any excess energy transfer from the H atom to a water molecule, above the elastic portion which goes initially into tranlational energy, would be absorbed by the water molecule in the form of a rotational (or vibrational) excitation. In most of the coma, which is optically thin in the infrared and where the intercollsion times between water molecules is very long compared with radiative lifetimes,

this excess tranferred energy would simply radiate away. The major effect would be on the more rapid thermalization of H atoms. This would result in a larger number of very low speed atoms than are evident (see Figure 6).

Inelastic collision cross sections are generally smaller than elastic cross sections (Bernstein, 1979). Such a generalization can also be inferred by the fairly long relaxation times required for polyatomic molecules to reach complete thermal equilibrium in their rotational and vibrational state distributions. For example up to 50 collisions are required for H_2 to reach rotational equilibrium, whereas thousands of collisions are required for triatomic molecules to reach vibrational equilibrium (Hirschfelder, Curtiss, and Bird, 1954). In addition, elastic cross sections are determined by using simple elastic models to interpret measured macroscopic quantities such as diffusion and viscosity, and thus likely incorporate some kind of average inelastic component at least in some implicit way. Therefore, our use of hard-sphere collisions to infer such macroscopic quantities as the energy transfer and velocity distribution of H atoms should at least be self-consistent. Similar reasoning is also employed in hydrodynamic models (Marconi and Mendis, 1983, 1984, and Gombosi et al. 1986) which use momentum transfer rates based on the same type of hard-sphere elastic collisions.

Another important implication of the reproducibility of the isophote contours by the extended coma MCTPM is that we have used the excess speed distribution for H atoms dissociated for OH radicals according to the ab initio calculations of van Dishoeck and Dalgarno (1984) who predict high lying predissociation states, with large excess energies yielding fast H atoms, having speeds of 17 to 26 km/s. If we ignore these newly identified states and consider all of the H atoms produced from OH only at 8 km/s (as is a common practice) the shapes of the modeled isophote contours deviate from the

observed shapes significantly. This result and the previously mentioned observation of the emission at 6300 Å from O(^{1}D) atoms at nearly 10^6 km from comet P/Halley by Roesler et al. (1987) would seem to verify the importance of these new predissociation transitions.

The fact that our model can directly account for the speed distribution of H atoms leaving the inner coma which successfully reproduces the Lyman-α isophotes has some important implications regarding the proper modeling of hydrogen in other situations. Keller and Meier (1980) also used the syndyname model in order to reproduce the observed Lyman-α images of comet West (1976 VI), but they required the presence of an outburst in the production of H at some past time. The comet West observation was, like Kohoutek, of a very productive comet (actually more productive) at a small heliocentric distance (0.4 AU) where collisions should be expected to be important in determining the exit speeds of H atoms from the inner coma. However, for comets either less productive than Kohoutek at small heliocentric distances, or as productive but at larger heliocentric distances, the role of collisions in shaping the effective exit speed distribution of H atoms from the inner coma would be minimal.

The effective speed distributions for H atoms in these essentially "collisionless" cases would be set by the proper vector sums of several components: (1) the speed from the excess energy of all photodissociations, (2) the outflow speed of the coma, and (3) the temperature of the coma gas. An example of such a "collisionless" speed distribution can be illustrated by the dashed histograms in Figure 6 which show the initial speed distributions of the H atoms in the Kohoutek models upon their initial production but before any collisions. Example models have been presented earlier (Combi and Smyth 1987) for the case of the rocket image of Kohoutek at 0.43 AU, where the

production rate was reduced by factors of 3 and 10, thereby reducing significantly the number and importance of collisions. The spatial character of the cloud also changed markedly for these cases. Previous MCPTM results published for the Pioneer Venus Orbiter UVS observations of comet P/Giacobini-Zinner made during the ICE encounter were made using an (appropriately) collisionless version of the model which should certainly be valid for this comet at 1.03 AU from the sun where the water production rate was only 2.3×10^{28} molecules per second (Combi, Stewart and Smyth 1986).

V. Discussion

The application of the MCPTM, described in a general mathematical form in the accompanying paper (Paper 1), has been applied in this paper to explain the observed spatial morphology of the Lyman-α coma. The two electrographic camera images of comet Kohoutek (1973 XII) were chosen for this particular study. Although these images had been reasonably well reproduced in the original observation paper by Meier et al. (1976), the physical basis of their sums of two or three Maxwell-Boltzmann distributions for the effective H atom radial outflow speeds remained unquantified. In this paper the MCPTM accounts explicitly for the time-dependent physical state of the inner coma source, the proper isotropic (vectorial) ejection of daughter OH radicals and H atoms, the collisional thermalization of the H atoms (which is generally only partial), and the explicit calculation of the trajectories of the appropriately produced H atoms under the influence of solar radiation pressure and gravity in three dimensions.

While a comparison of the multi-component Maxwellian distributions of Meier et al. with the effective outflow speed distributions of H atoms from the inner coma as modeled by the MCPTM shows clear differences in the detailed appearance, there is enough broad similarity to see why both models can produce a reasonable fit to the data. The success of the physically-based MCPTM, however, implies that the models of Keller and Meier (1976) cannot be applied indiscriminately to the hydrogen observations of comets other than very productive comets at small heliocentric distances. In fact, the reason the multi-component Maxwellian models are successful is simply due to the observational selection effect that only very productive comets at small heliocentric distances have been observed in a manner which yield the wide field images available for comets Kohoutek and West. Furthermore, it is only

for comets at small heliocentric distances that the radiation pressure is large enough so that appropriate modeling is particularly sensitive to the effective outflow speed distribution of H atoms from the inner coma.

It is important to stress that we have been able to produce an effective time-dependent outflow speed distribution of H atoms leaving the inner coma which successfully reproduces the observed Lyman-α isophote gradient and shapes, using an inherently physically-based self-consistent model. Although many processes were included in the model, and best estimates had to be made for a number of physical parameters, there are few truely free fitting parameters in the entire procedure. Sensitivity studies of the important parameters would certainly represent interesting, although somewhat computationally intensive, future undertakings. Apart from this there are two important areas for future improvements and generalizations which can be made to the model and the modeling process.

In the details of the collision calculation, an obvious improvement would be to include the exact expression for the collision path integral (Eq. 31, in Paper 1). Although for the first several collisions, where an atom's speed is large compared with the outflow speed and where the bulk of the heating takes place, the approximate expression (Eq. 32 in Paper 1) is clearly a reasonable choice. After a number of collisions, the atoms are more or less thermalized, and the exact expression for the collision path is more appropriate. However, it will not make much difference to the final atom kinematics if the atoms are collided a few too many times once they are already thermalized. Another improvement in the area of the collision process is to carefully consider the applicability of the oversimplified hard-sphere scattering which has always been used (and is here) in order to understand the role of collisions between atoms, radicals and molecules.

The more fundamental direct improvements are to be made to the physical inner coma description. The possible effect of dust, plasma, and the minor heating mechanisms should be addressed more carefully. The collisional decoupling of the hot H atoms from the heavier coma gas molecules represents a first order correction to the general problem of the breakdown of fluid mechanics in describing not only the correct photochemical heating but more generally the physics of the outflow of the cometary coma. A better treatment of the problem would be accomplished by including separate MCPTM calculations for each of the important species, namely H, OH, O, H_2O, CO and CO_2. In this way not only can a complete description for observable species be made, but also, a basic study at the kinetic theory level of the breakdown of the applicability of fluid mechanics could be studied.

Acknowledgements

Support for this research was provided by contracts NASW-3950 and NASW-3966 from the Planetary Atmospheres program at NASA. The careful and patient reading of this paper by an anonymous referree, and the constructive comments are gratefully acknowledged.

References

Allen, C.W., 1973, Astrophysical Quantities, Oxford University Press, London.

Balsiger H., et al., 1986, Nature, 321, 330.

Bernstein, R.B., 1979, "Atom-Molecule Collision Theory," Plenum Press, New York, p. 30.

Combi, M.R., 1987, Icarus, to appear July 1.

Combi, M.R. and Delsemme, A.H., 1980, Ap. J., 237, 633.

Combi, M.R., and Smyth, W.H., 1987a, Proc. Symp. on the Diversity and Similarity of Comets, ESA SP-278, in press.

Combi, M.R., and Smyth, W.H., 1987b, Ap. J., companion paper this issue.

Combi, M.R., Stewart, A.I.F. and Smyth, W.H., 1986. GRL, 13, 385.

Crovisier, J., 1984, Astr. Ap., 130, 361.

Delsemme, A.H., 1973, Space Sci. Rev., 15, 89.

Delsemme, A.H., 1976, in Comet Kohoutek, ed. by G.A. Gary, NASA SP-355, 195.

Feldman, P.D., A'Hearn, M.F., Festou, M.C., McFadden, L.A., Weaver, H.A., and Woods, T.N., 1986, Nature, 324, 433.

Festou, M.C., 1981a, Astr. Ap., 95, 69.

Festou, M.C., 1981b, Astr. Ap., 96, 52.

Festou, M., Jenkins, G.B., Keller, H.U., Barker, E.S., Bertaux, J.L., Drake, J.F. and Upson, W.L., 1979, Ap. J., 223, 638.

Gombosi, T.I., Nagy, A.F., and Cravens, T.E., 1986, Rev. Geophys. 24, 667.

Hirshfelder, J.O., Curtiss, C.F., Bird, R.B., 1954, "Molecular Theory of Gases and Liquids," Wiley & Sons, New York, p. 21.

Huebner, W.F. and Keady, J.J., 1983, International Conference on Cometary Exploration, Hungarian Academy of Sciences.

Huppler, D., Reynolds, R.J., Roesler, F.L., Scherb, F., and Trauger, J., 1975, Ap. J. (letters), 202, 276.

Ip, W.-H., 1983, Ap. J., 264, 726.

Johnson R.E., 1982, "Introduction to atomic and molecular collisions", Plenum Press, New York, 19.

Keller, H.U., and Lillie, C.F., 1974, Astr. Ap., 34, 187.

Keller, H.U. and Meier, R.R., 1976, Astr. Ap., 52, 273.

Keller, H.U. and Thomas, G.E., 1975, Astr. Ap., 39, 7.

Krankowsky, D., et al., 1986, Nature, 321, 326.

Larson, H.P, Davis, D.S., Mumma, M.J., and Weaver, H.A., 1986, Ap. J. (Letters), 309, L95.

Lean, J.L., and Skumanich, A., 1983, JGR, 88,5751.

Lemaire, P., Charra, J., Jouchoux, A., Vidal-Madjar, A., Artzner, G., Vial, J.C., Bonnet, R.M., and Skumanich, A., 1978, Ap. J. (Letters), 203, 509.

Marconi, M.L. and Mendis, D.A., 1983. Ap. J., 273, 381.

Marconi, M.L. and Mendis, D.A., 1984, Ap. J., 287, 445.

Marconi, M.L. and Mendis, D.A., 1986, The Moon and Planets, 36, 249.

McElroy, M.B., and Yung, Y.L., 1975, Ap. J., 196, 227.

Meier, R.R., and Keller, H.U., 1980, Astr. Ap, 81, 210.

Meier, R.R., Opal, C.B., Keller, H.U., Page, T.L., Caruthers, G.R., 1976, Astr. Ap., 52, 283.

Roesler, F.L., Scherb, F., Magee-Sauer, K., Harlander, J., 1987, pre-preint.

Schleicher, D.G., 1983, Ph.D. thesis, University of Maryland.

Schleicher, D.G., and A'Hearn, M.F., 1984, B.A.A.S., 15, 806

Slanger, T., 1982, private communication.

van Dishoeck, E.F., and Dalgarno, A., 1984, Icarus, 59, 305.

TABLE 1

Photoabsorption of Solar UV Radiation by H_2O Vapor

Wavelength Range	Reaction	Product Velocities (km sec^{-1})		Fraction of Total H_2O Photoabsorbed	
		H Atom	OH Molecule	Quiet sun	Active sun
1357Å < λ < 1860Å	$H_2O + h\nu \rightarrow H + OH(X^2\Pi)$	20	1.2	.670	.534
	$\rightarrow H_2 + O(^1D)$	—	—	.007	.005
λ = 1216Å	$H_2O + h\nu \rightarrow H + OH(X^2\Pi)$	30	1.8	.167	.269
	$\rightarrow H_2 + O(^1D)$	—	—	.023	.036
	$\rightarrow H + OH^*(A^2\Sigma^+) \rightarrow H + O + H$	$\leq$ 5.0	—	.027	.044
	$\rightarrow H + OH(A^2\Sigma^+)$	5.0	0.3	.009	.015
984Å < λ < 1357Å	$H_2O + h\nu \rightarrow H + OH(X^2\Pi)$	25–35	1.2–2.0	.028	.021
	$\rightarrow H_2 + O(^1D)$	—	—	.004	.003
	$\rightarrow H + OH^*(A^2\Sigma^+) \rightarrow H + O + H$	4.0–6.0	—	.004	.003
	$\rightarrow H + OH(A^2\Sigma^+)$	0–17.0	0–1.0	.002	.001
λ < 984Å	$H_2O + h\nu \rightarrow$ ionization products [H_2O^+, etc.]	—	—	.059	.069

TABLE 2

Photoabsorption of Solar UV Radiation by OH[(a)]

Wavelength	OH Predissociation State	H Atom Velocity ($km\ s^{-1}$)	Photodissociation Rate ($10^{-6}\ s^{-1}$)	
			Active Sun	Quiet Sun
2160Å	$A^2\Sigma^+(v' = 2)$	8	3.0-6.1[(b)]	3.0-6.1[(b)]
2450Å	$A^2\Sigma^+(v' = 3)$	11	0.5	0.5
1400Å<λ<1800Å	$1^2\Sigma^-$	22-26	2.3	1.4
1216Å	$1^2\Delta$	26.3	0.75	0.3
1216Å	$B^2\Sigma^+$	17.1	0.13	0.05
1216Å	$2^2\Pi - 3^2\Pi$	26.3	0.25	0.10
1200Å	$D^2\Sigma^-$	22	<0.01	<0.01

(a) Rates and Branching Ratios - van Dishoeck and Dalgarno (1984)

(b) Heliocentric Velocity Dependence - Schleicher (1983)

TABLE 3

Coupled Gas - Dynamic/MCPTM

Heliocentric Distance (AU)	Water Production Rate[d] (s^{-1})	Initial Gas[e] Temperature (K)
0.434[a]	8.8×10^{29}	208
0.25[a]	2.7×10^{30}	216
0.142[b]	6.4×10^{30}	225
0.25[c]	2.5×10^{30}	216
0.434[c]	5.5×10^{29}	208

[a]pre-perihelion

[b]perihelion

[c]post-perihelion

[d]Based on $Q_o = 1.47 \times 10^{29}$ s^{-1} at 1 AU pre-perihelion in Figure 2.

[e]Extrapolated from Gombosi et al. (1985)

Figure Captions

Figure 1. Solar Lyman-α Line Profile. The full solar disc Lyman-α line profile as adopted in the MCPTM was constructed by Lemaire et al. (1978) from high resolution disc-centered and limb spectra. The geocoronal absorption at line center was filled-in to approximate the flux as seen by a hydrogen atom in the cometary coma.

Figure 2. Variation of the Relative Gas Production Rate in Comet Kohoutek. The heliocentric distance dependence of the relative gas production rate as adopted from the visual light curve of comet Kohoutek which was compiled by Delsemme (1976). The variation is normalized to the production rate at 1 AU pre-perihelion. The circles show the pre-perihelion values, while the stars show the post-perihelion values.

Figure 3. Five Coupled Gas-dynamic/MCPTM Coma Results for Comet Kohoutek. Shown are the temperature, outflow speed, and Mach number of the coma gas as a function of radial distance to the nucleus. The dashed curves show the model results for the pre-perihelion heliocentric distances indicated, whereas the solid lines give the post-perihelion results. The coma model parameters are given in Table 3 and all model curves are terminated at the boundary of the collision zone radius.

Figure 4. MCPTM/Data Comparison of the Lyman-α Coma of Comet Kohoutek at 0.43 AU. The isophote contours for the data (solid lines) as observed by Meier et al. (1976) are compared with the fully time-dependent 3D self-consistent MCPTM result (dashed lines). The contours are in units of kiloRayleighs and the tick marks on the circumscribed box are separated by 1.25×10^6 km.

Figure 5. MCPTM/Data Comparisons of the Lyman-α Coma of Comet Kohoutek at 0.18 AU. The isophote contours for the data (solid lines) as observed by Meier et al. (1976) are compared with the fully time-dependent 3D self-consistent MCPTM result (dashed lines). Part (a) shows the optically thin result, and part (b) shows the result of a simple plane parallel radiative transfer correction (T=5000K) to the thin case. A true spherical radiative transfer calculation which takes the real phase space distribution (density and velocity) into account should fall intermediately between these two models. The contours are in units of kiloRayleighs and the tick marks on the circumscribed box are separated by 4.0×10^5 km.

Figure 6. A Comparison of the Velocity Distribution Functions for H atoms Leaving the Inner Coma in the MCPTM and Syndyname Model. The smooth solid curves show the sums of the three-component Maxwellians of the syndyname models of Meier et al. (1976). The solid histograms give the MCPTM distribution functions for H atoms leaving the inner collisional coma and transition zone. The dashed histograms give the MCPTM distribution functions for the H atoms upon initial production at dissociation of the parent H_2O molecules and OH radicals but before collisions. Part (a) gives the results for comet Kohoutek at 0.18 AU, and part (b) gives the results at 0.43 AU.

Michael R. Combi and William H. Smyth

Atmospheric and Environmental Research, Inc.

840 Memorial Drive

Cambridge, MA 02139-3758

Full Solar Disk Lyman-α Line Profile

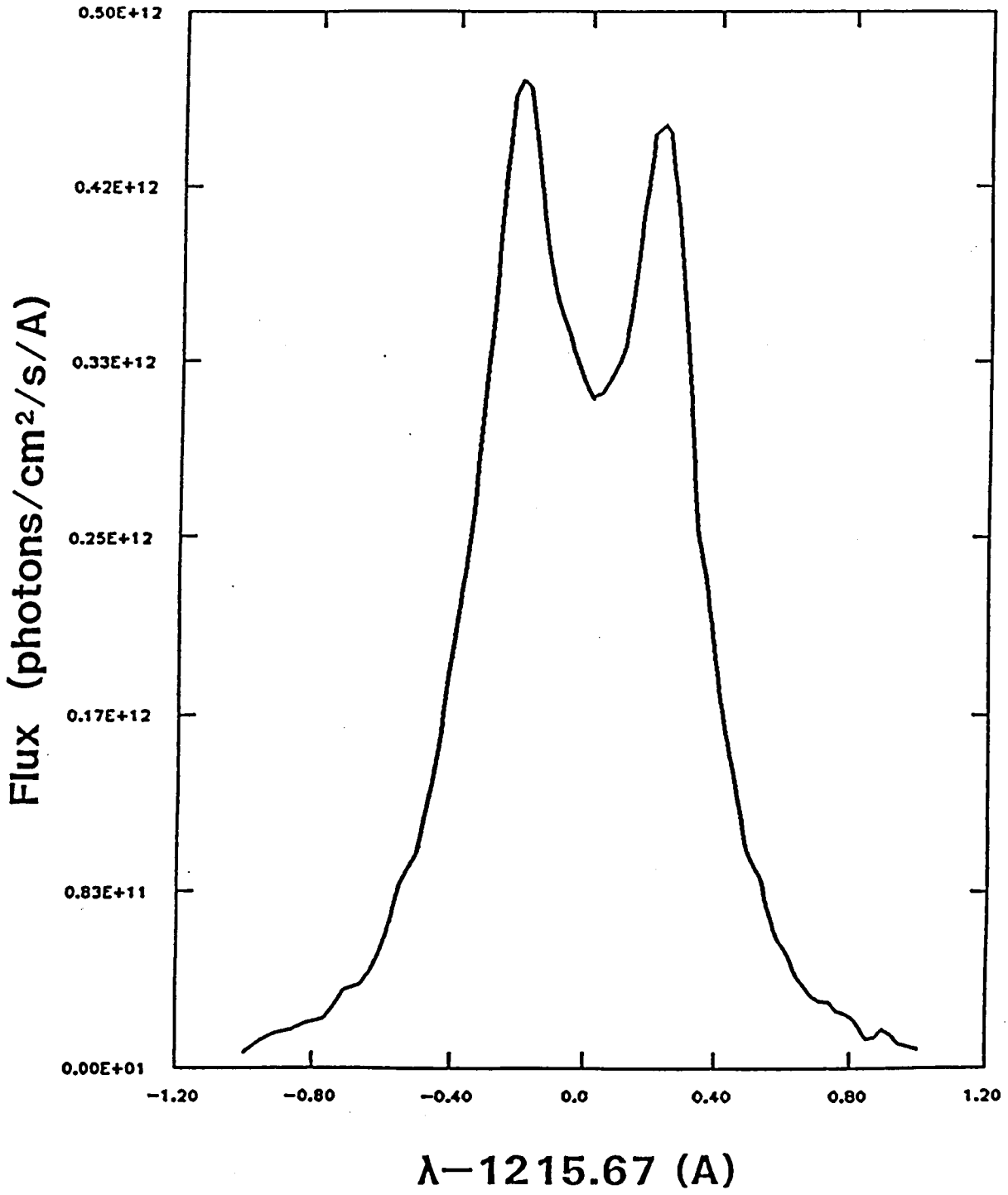

FIGURE 1

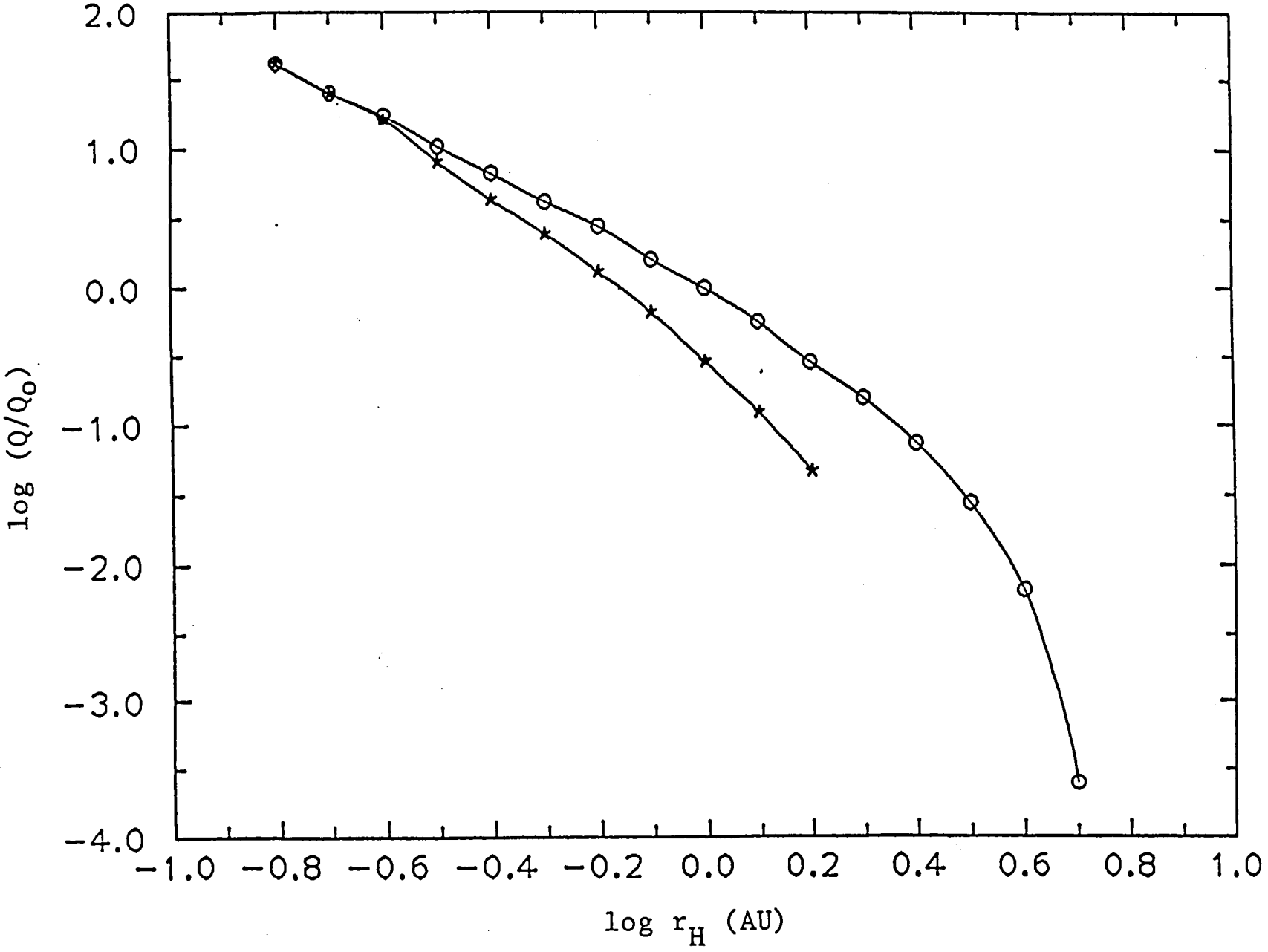

FIGURE 2

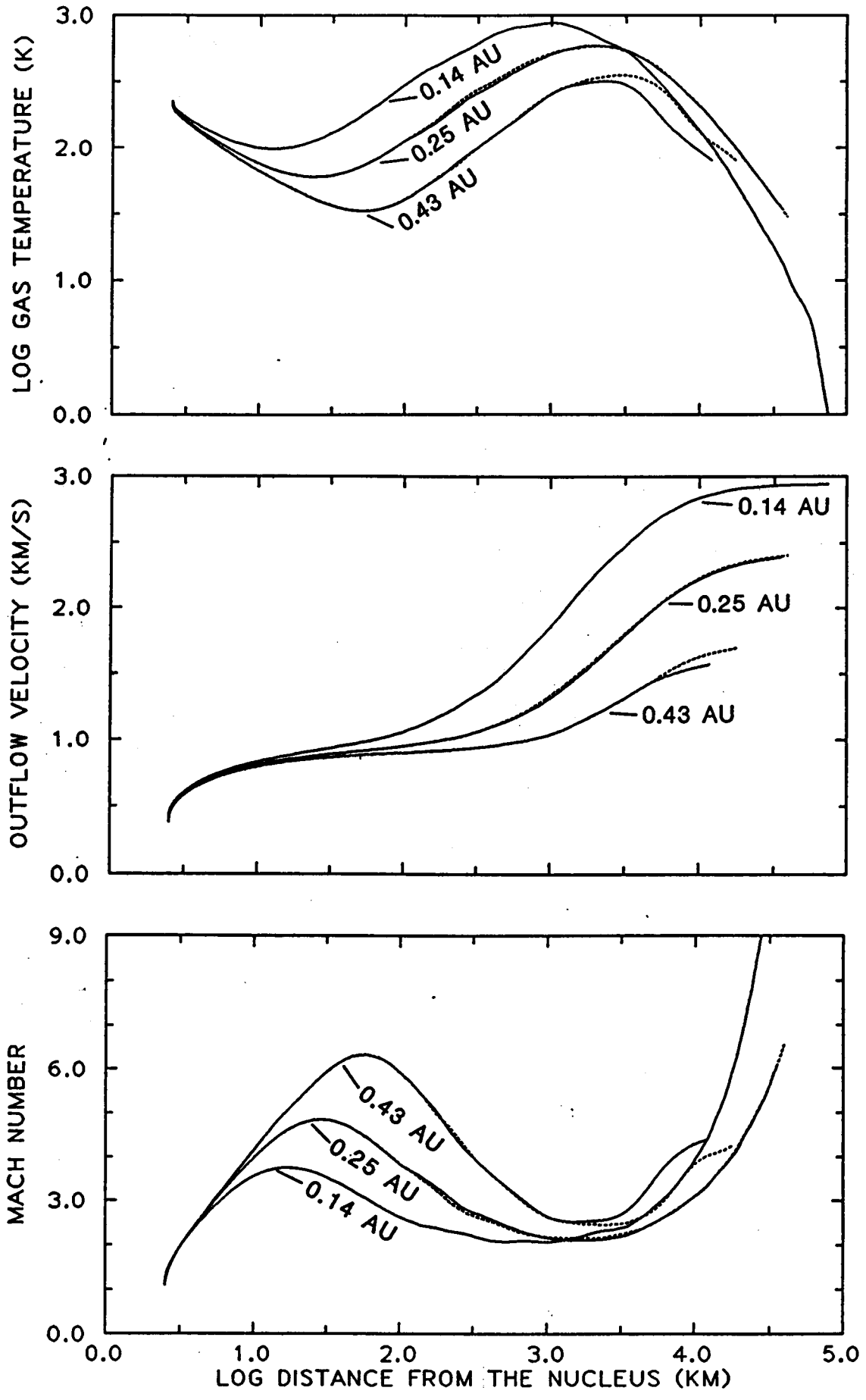
LOG GAS TEMPERATURE (K)
3.0
2.0
1.0
0.0
0.14 AU
0.25 AU
0.43 AU
OUTFLOW VELOCITY (KM/S)
3.0
2.0
1.0
0.0
0.14 AU
0.25 AU
0.43 AU
MACH NUMBER
9.0
6.0
3.0
0.0
0.43 AU
0.25 AU
0.14 AU
0.0
1.0
2.0
3.0
4.0
5.0
LOG DISTANCE FROM THE NUCLEUS (KM)

FIGURE 3

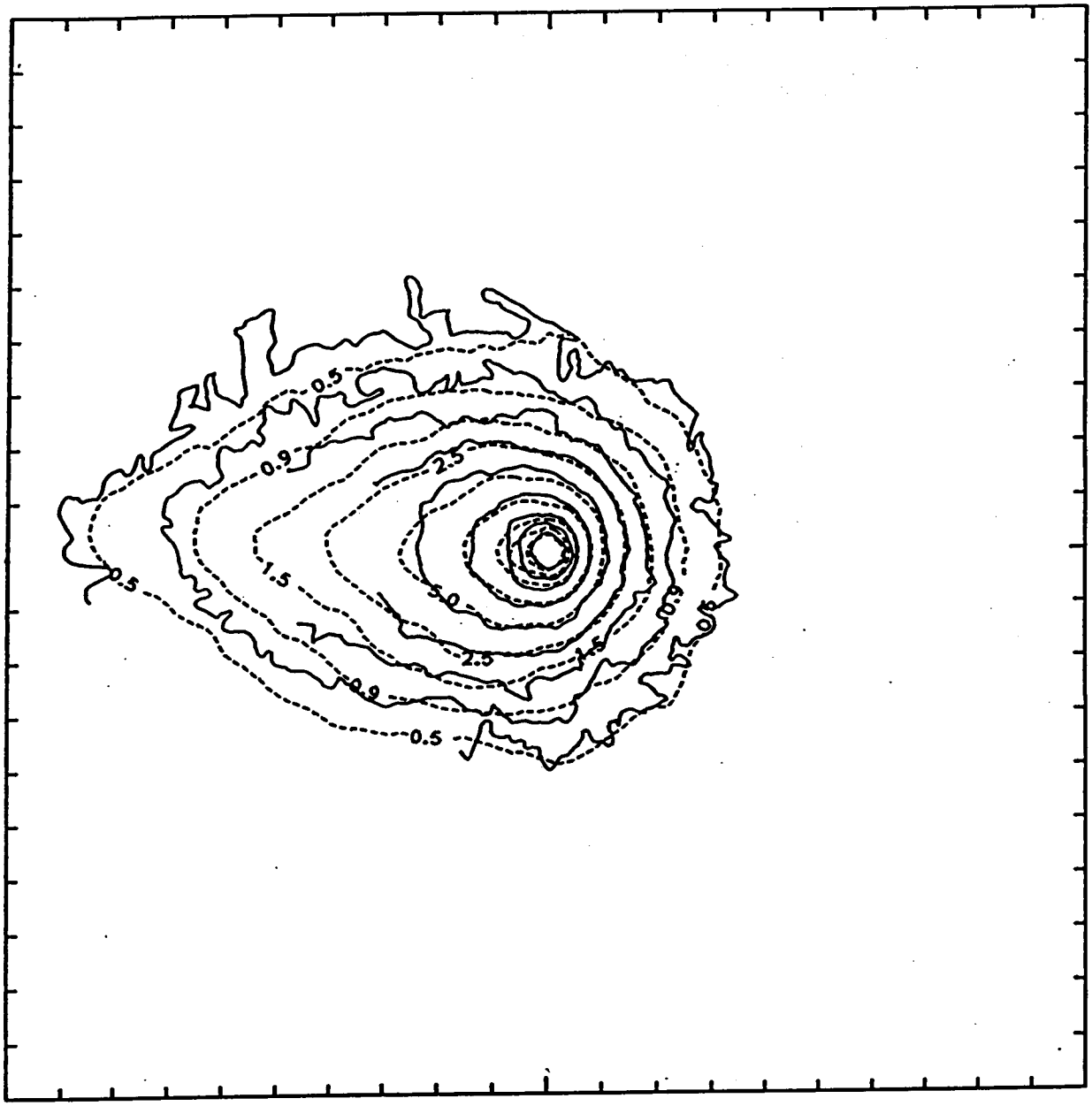

FIGURE 4

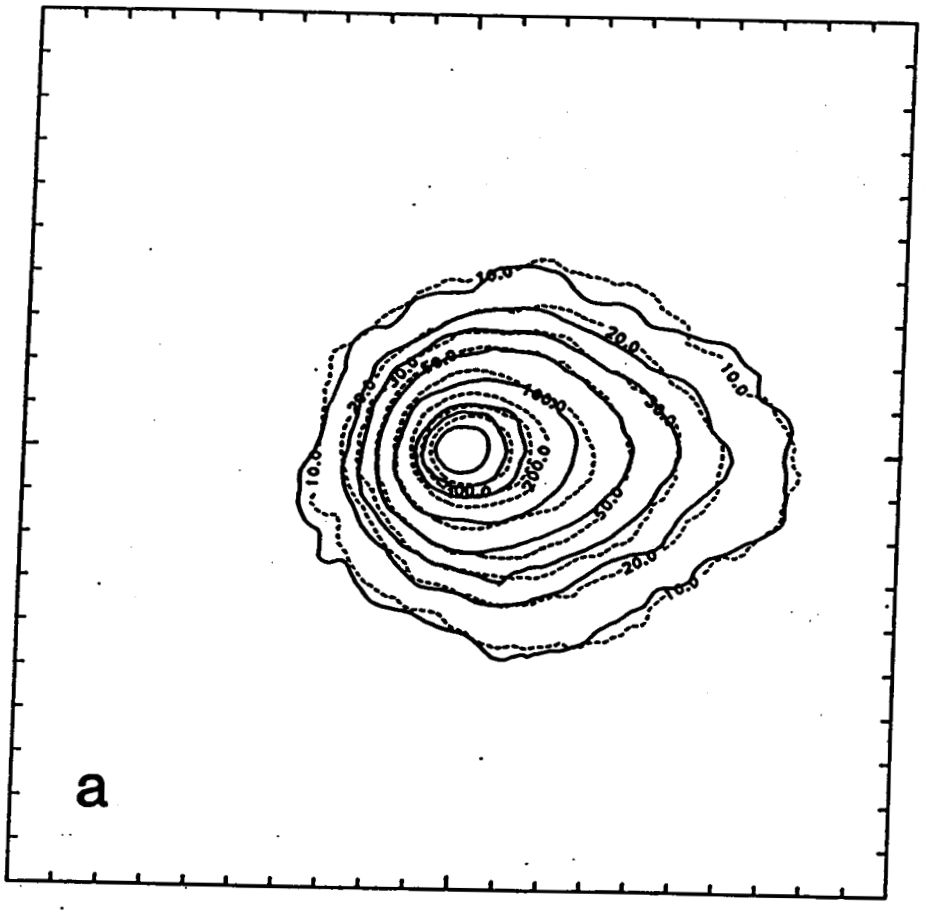
10.0
20.0
30.0
50.0
100.0
200.0
300.0
a

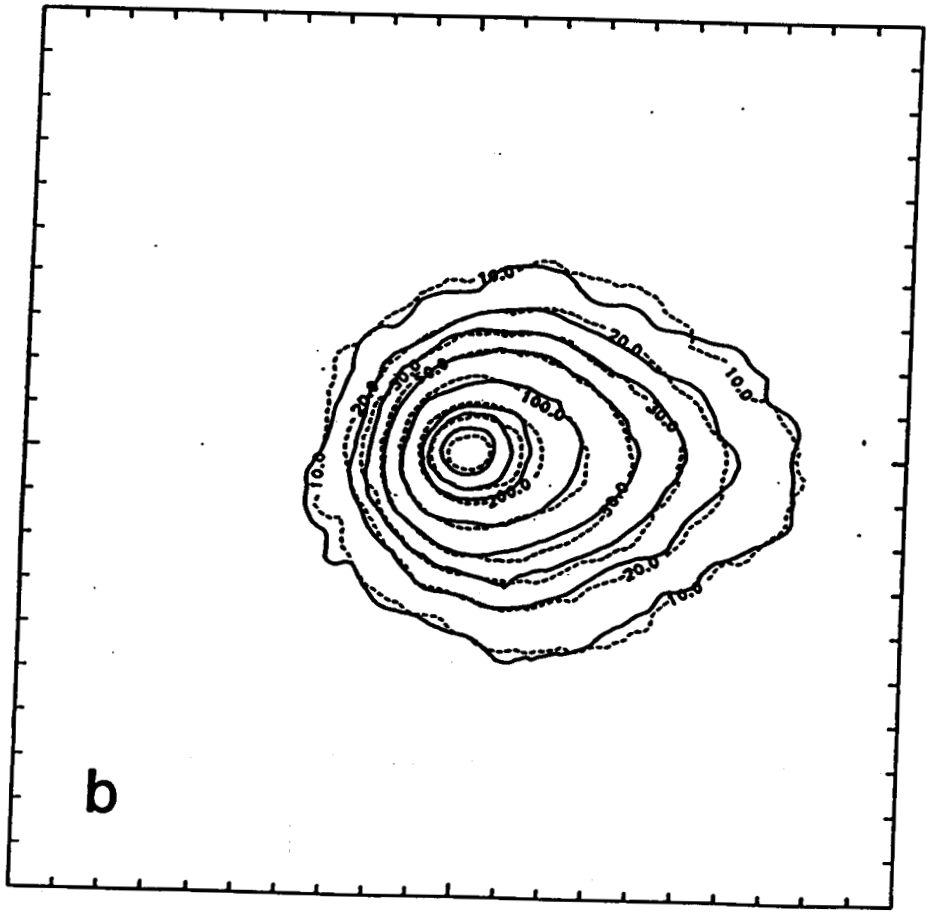
10.0
20.0
30.0
50.0
100.0
200.0
300.0
b

FIGURE 5

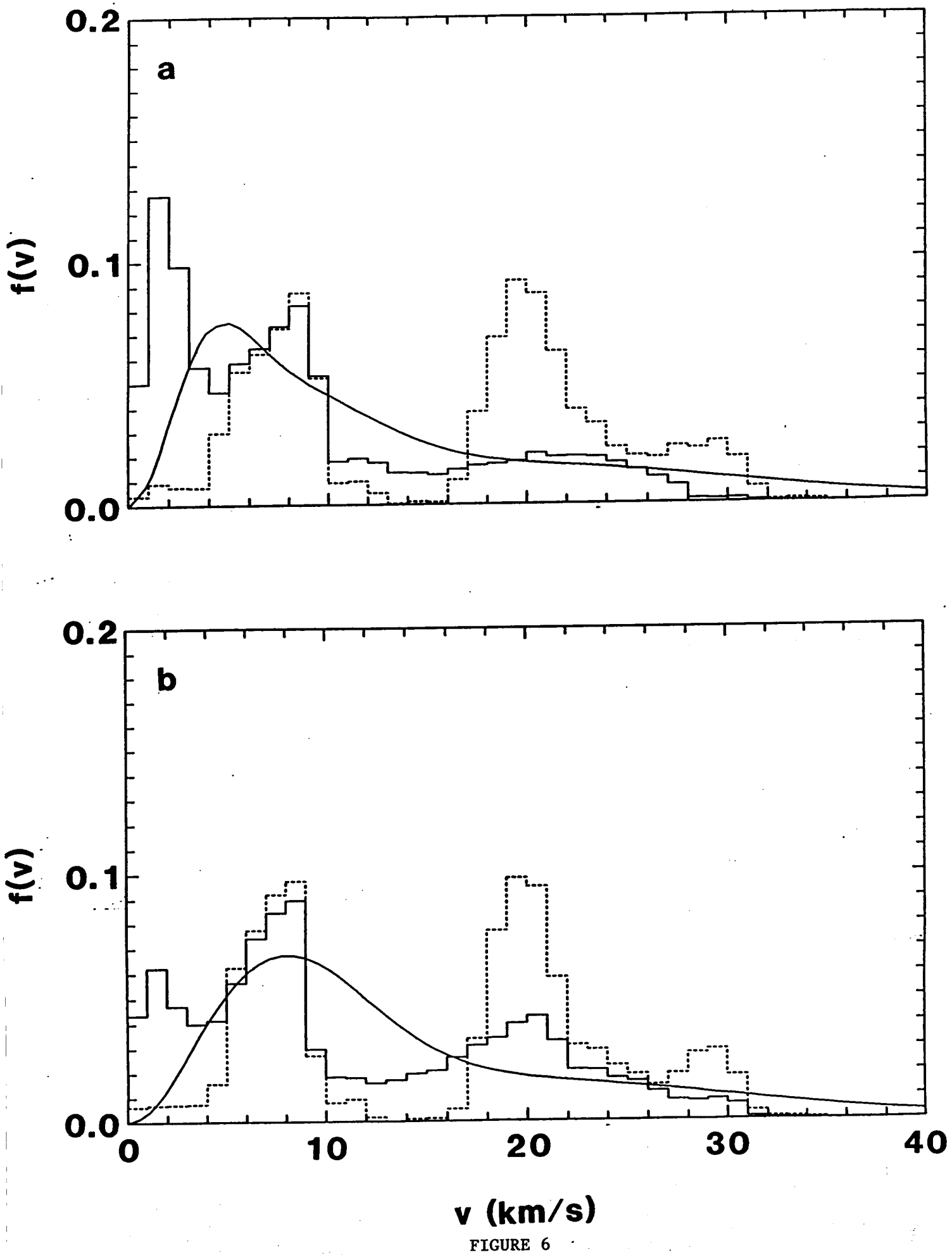

FIGURE 6